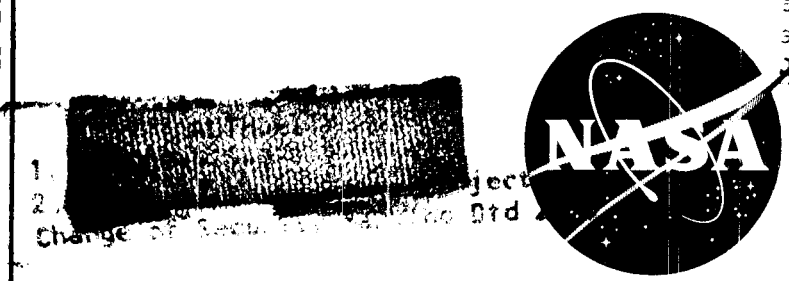

TECHNICAL MEMORANDUM

X-197

EXPERIMENTAL INVESTIGATION OF A TRANSONIC COMPRESSOR

CASCADE AND TEST RESULTS FOR FOUR BLADE SECTIONS

By James C. Emery, James C. Dunavant,
and Willard R. Westphal

Langley Research Center
Langley Field, Va.

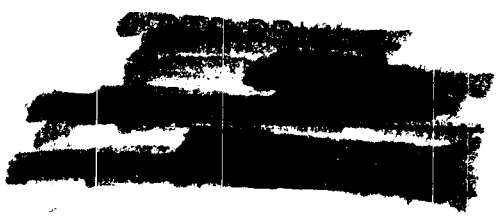

NATIONAL AERONAUTICS AND SPACE ADMINISTRATION

WASHINGTON

January 1960

NATIONAL AERONAUTICS AND SPACE ADMINISTRATION

TECHNICAL MEMORANDUM X-197

EXPERIMENTAL INVESTIGATION OF A TRANSONIC COMPRESSOR CASCADE AND TEST RESULTS FOR FOUR BLADE SECTIONS*

By James C. Emery, James C. Dunavant,
and Willard R. Westphal

SUMMARY

This investigation describes the development of a transonic compressor cascade and includes test results for four blade sections over a range of Mach number from 0.7 to 1.4.

The results indicate that a transonic cascade is practical and will give much needed information applicable to compressor design. Cascade pressure rise is shown to be in agreement with the single-rotor test point which is available.

INTRODUCTION

Large gains in compressor pressure ratio and mass flow have been achieved at reasonable efficiency by using transonic velocities relative to the blades (ref. 1). Many such experimental compressors have been investigated, and compressors having transonic velocities in portions of the first stages are operationally in use. Reported results of transonic compressor overall performance and blade-section performance are readily available. However, detailed study of the flow between the blades is naturally extremely difficult on rotating blades, even though techniques for measuring pressure distribution, visualizing the flow through schlieren and shadowgraph techniques, and hot-wire measurements have been developed.

For subsonic velocities, the cascade provided a convenient means for study of flows and design performance of blade sections at near-sonic entering Mach numbers. The logical extension of subsonic-cascade operation into the transonic region was prevented by choking in the

*Title, Unclassified.

entrance region between the blades and the tunnel wall. For wind-tunnel testing, the use of a slotted-wall section along the tunnel wall as a means of smoothly accelerating the air just above the speed of sound proved a feasible means of avoiding the effects of choking. This principle is here applied to cascades.

Many other problems appeared and required study. The more difficult of these is the mechanism of the flow in the entrance region caused by the inability of the transonic cascade to simulate an infinitely long cascade. Kantrowitz described, in reference 2, the wave patterns which would exist in a supersonic, infinitely long cascade. Waves from each blade would presumably extend an infinite distance from this cascade were it not for the attenuating effects between the expansions and compressions as the distance from the blades increased. The transonic cascade can only simulate the flow of the infinitely long cascade to the extent possible with a practical number of blades which, because of the high power required, are very few in number.

The transonic cascade is inherently different from the subsonic cascade, which has end fairings designed to produce uniform flow from top to bottom of the cascade. Several blades will be required in the transonic cascade to set up a flow field which for a portion of the blade row simulates the flow of an infinite cascade.

The present investigation was undertaken at the Langley Research Center of the NASA to determine experimentally the feasibility of the design and the problems associated with the transonic cascade. A 7-inch high-speed-cascade tunnel at the Langley Research Center was modified by adding a slotted floor connected to a suction system. Four blade sections were tested, one being of conventional compressor-blade design and others of special design.

The present paper is a brief summary of experiments and results obtained in the transonic-cascade program. Unfortunately, the program was terminated before the complete practical solution of a transonic cascade could be accomplished. However, the results presented herein are believed to demonstrate that the transonic cascade is feasible.

SYMBOLS

$c_{l,o}$ camber, expressed as a design lift coefficient of isolated airfoil

M Mach number

$\overline{M}$ average Mach number

p	pressure
q	dynamic pressure, $\rho V^2/2$
$\left(\frac{\Delta p_t}{q_1}\right)_{av}$	average total-pressure-loss coefficient
V	velocity
x	distance parallel to blade chord
y	distance perpendicular to blade chord
α	angle of attack
β	inlet airflow angle
θ	turning angle
ρ	mass density
σ	solidity (ratio of blade chord to gap between blades)
c	chord

Subscripts:

1	upstream of blade row
2	exit of blade row
t	total, stagnation
b	blade

APPARATUS AND METHODS

A 7-inch high-speed-cascade tunnel at the Langley Research Center described in reference 3 was modified by adding a slotted floor to attain transonic speeds. A schematic cross section of the modified tunnel is shown in figure 1. Slots designed to produce a range of transonic Mach numbers in wind tunnels are described in many reports; for instance, in reference 4. The Mach number is varied by removing a portion of the flow through slots in the tunnel walls. A second effect

of the slots is to maintain a near constant static pressure in the direction of the flow, thereby tending to reduce the strength of shocks, reflections, choking, or velocity changes in the flow.

Eight slots parallel to the flow direction and extending from a point just behind the inlet fairing to the blade package were cut in the upper floor. The area of the slots was determined from reference 4. The open area of the slots (fig. 2(a)) was found to be insufficient in early tests and, hence, the open area of the slot was doubled. The final slot configuration shown in figure 2(b) consisted of eight 36-inch openings tapered to zero width at the upstream end. The open area of the slots comprised about 30 percent of the cross-sectional area of the top floor. An enclosed chamber was placed behind the slots and connected to the exhaust blower. This blower was a rotary positive-displacement pump rated at 10,000 cubic feet per minute and limited to a pressure ratio of 2. Discharge was to the atmosphere. Boundary-layer buildup on the test-section side walls greatly increases the actual volume over the theoretical volume, which must be removed to produce a given Mach number; and blower capability limited the tunnel upstream Mach number to 1.25 with straight floors.

In order to lessen the required amount of flow removed through the slots, the flat lower floor was made adjustable so that it could be shaped to form an $M = 1.3$ nozzle. (See fig. 1.) The floor was kept flat except at high Mach numbers where additional suction was necessary. To prevent boundary-layer buildup, the lower floor was made porous and the boundary layer was removed by a second vacuum system. On the tunnel side walls, protruding boundary-layer-removal slots (fig. 1) were also used to control the boundary layer as in previous subsonic cascade testing. These slots were also connected to the vacuum system and independently controlled.

Fairings (fig. 1) were used at the ends of the upper and lower floors to control the flow at the ends of the cascade. The adjustable lower-floor extension was made porous and the boundary layer removed to prevent separation. The upper floor, having a less critical pressure-rise condition, was not porous but was adjustable.

In the tests of a cascade in which the side walls converged through the blade package, the geometric shapes required to permit adjustment to the floors were so complex that an alternate system was used. In this system, suction chambers were provided to remove all the flow between the walls and the upper and lower blades via the side-wall suction system. This system taxed the capacity of the side-wall suction system and was only used in the converging-wall cascade tests.

Side walls of the test section made entirely of glass were used in order that schlieren observation could be made over the entire length

of the cascade. The upstream flow distribution, especially at the end blade for the transonic cascade, was most critical; and during testing viewing of the flow by schlieren was the most practical and successful means of quickly estimating the uniformity of the flow in order to take corrective measures.

For subsonic-cascade operation a row of static-pressure orifices was contained in the side walls about two blade chords upstream of the blade row designated station A in figure 1. For transonic operation the orifices were located quite close to the blade row, about one-half chord upstream in the glass walls. These, however, were not included in the first blade package tested, the converging-wall tests. In all other blade tests the orifice locations are clearly visible in the schlieren photographs. The total pressure was measured from a pitot tube upstream of the nozzle in the settling chamber. A conventional total-pressure rake was mounted downstream of the blade row for downstream total pressure. Static-pressure taps were contained in the center blade at midspan. Downstream static pressure was obtained from the average of the wall pressure-orifice pressures located as shown in figure 1.

One cascade was tested with cascade side walls converging from 7 inches in span approximately 1/2 inch upstream of the blade row to 6 inches in span at a point 1/2 inch downstream of the blade row, thereby requiring a less critical pressure-rise condition for the cascade. The upstream bend in the glass walls can be seen in the schlieren photographs for this cascade. In testing the converging-wall blade package, which had no provision for measuring static pressures close to the cascade, difficulty was experienced in determining the upstream Mach number. An attempt was made to measure flow direction and Mach number from intersections of Mach waves from small disturbances placed in the tunnel. Small bead chains were mounted about 2 inches on either side of the center line to generate small shocks, and these may be seen in many of the schlieren photographs.

BLADE TESTS AND PRESENTATION OF RESULTS

Blade Sections

In order to decrease pressure rise on the blade upper surface, blade sections have been designed in the forward portion with very little surface curvature and with the loading on the surface of highest curvature on the rearward portion of the blade; consequently, two blades were designed by combining these features. The blade section designated T1-$\left(8A_2I_{8_b}\right)$06 (ref. 1) has the maximum thickness located at

the 65-percent-chord point as compared to the 40-percent-chord point for the NACA 65-series thickness distribution frequently used for subsonic compressor blading. The coordinates for this thickness distribution are given in table I and a comparison with the 65-series thickness distribution is presented in figure 3 for a maximum thickness of 6 percent. This section was tested in a transonic rotor and the results are given in references 1 and 5. The convergence of the cascade walls in tests of this blade section was designed to duplicate the axial-velocity change which occurred in the rotor tests.

The second blade section, referred to as blade CW_1, has a 5° wedge at the leading edge, a flat bottom, and a circular-arc trailing-edge airfoil section and is shown in figure 4 along with construction dimensions for a maximum thickness of 6.3 percent. The third blade section was CW_1 reversed, trailing edge to leading edge, and is referred to as the CW_2 blade section.

A fourth airfoil, the 65-$(4A_{10})$06, has been frequently used for high-speed and compressor-tip sections, and was tested primarily for comparative purposes. The coordinates for this airfoil are given in table II.

All airfoils were of 2.8-inch chord. Reynolds number based on chord at $M_1 = 1.0$ is 1.4×10^6 and is above the value where compressor blades have been known to exhibit Reynolds number effects.

Presentation of Results

Performance of the blade section is presented in tabulated form in figures 5 to 25, and table III tabulates conveniently the various configurations. Data at the higher inlet-air angles are presented in figures 5 to 14 and at the lower inlet-air angles in figures 15 to 25. Each figure is composed of four schlieren pictures and four corresponding tables, each one of which represents a different entering Mach number. The tabulated portion of each of figures 5 to 25 presents the Mach number distribution taken from the static orifices in the glass wall $\overline{M}_1$ (side-wall orifice locations are shown in the schlieren photographs), the surface Mach number on the middle blade in the cascade M_b, the average total-pressure-loss coefficients, and the average exit Mach number $\overline{M}_2$. The tabulated blade surface Mach numbers M_b begin near the trailing edge of the blade on the pressure surface and continue around the blade clockwise at various chordwise positions. The Mach numbers are calculated by assuming no total-pressure loss. Figures 26 to 30, inclusive, present comparative pressure-rise and

pressure-loss values against Mach number for several of the configurations investigated.

DISCUSSION OF TEST RESULTS

Test Section Flow

Upstream flow region.- Expansions or compressions from the blades of the cascade are propagated only in a region bounded by the leading-edge shock of the first blade in cascade. Kantrowitz has shown in reference 2 that the compression and expansion waves upstream of an infinite cascade or rotor emanating from each blade must cancel, and the upstream Mach number will be that of the flow in the region where the waves are cancelled. In the transonic cascade the upstream region influenced by the blades is limited by the bow wave of the first blade and the tunnel wall above the blades. The leading edge of the first blade in cascade is, in effect, in an isolated flow field uninfluenced by any preceding blade. The flow field generated by the upper surface of the first blade in cascade encompasses all the remaining blades and probably changes both the Mach number and flow direction for all the remaining blades. Similarly, the second blade influences the remaining blades in cascade, but to a different degree because the flow field at the leading edge of the second blade is in the local flow field of the first blade. Thus, the first several blades in cascade set up a flow field themselves as the expansions and compressions emanate from the leading edge and upper surface. The disturbances emanating from blades behind other blades will neutralize expansion with compressions, as shown by Kantrowitz in reference 2.

Plots of supersonic flow field using the method of characteristics in the leading-edge region indicate that the flow fields of blades after the first two are, for practical purposes, identical. The change in the leading-edge flow may be observed in many of the schlieren photographs shown; for instance, figures 13(c), 15(b), and 16. Note that the leading-edge shock off the first blade stands farther ahead of the blade and is nearer to normal than those off of the other blades. This result is to be expected because the expansions from the first blade have increased the Mach number.

In the transonic cascade uniform upstream flow conditions such as would exist far upstream of an infinite cascade or rotor are never attained because the area upstream of the cascade is limited. Hence upstream pressure and Mach number measurements are made in a region of changing Mach number due to the local influence of the blades. Largely for this reason, readings from individual pressure orifices have been tabulated in the figures. Where an upstream Mach number has been used

in this report, it was determined from the average of the pressure orifices behind the bow shock of the first blade in cascade.

A primary cause for choking was the critical setting and shaping of the lower-floor fairing. As for the blade passages, the passage between the lower floor and the first blade must diverge from the blade leading edge rearward. It was observed that if a convergence exists in this passage, the passage entrance will be subsonic and the shock strong. Flow from this high-pressure region will spill over the leading edge of the first blade and cause the upper portion of the bow shock to be stronger for this blade than for the remaining blades. When the passage between the lower floor and the first blade is excessively open, flow separated from the lower floor. This separated region constituted a blockage which caused the flow to curve over the first blade. Experience has shown that the best condition of the lower floor is that it begin curving ahead of the first blade, that the passage be less than half a gap and smoothly diverging, and that the boundary layer be removed through the floor by making it porous.

At the top of the cascade a normal shock occurred between the upper floor and the last or next-to-last blade. (See figs. 10(b), 10(d), and 19(d), for example.) Improvements might be made in the flow in this region; however, as yet this region has received insufficient attention.

Blade Model Tests

Variation of pressure-rise and pressure-loss coefficients with Mach number is shown in figure 26 for the T1-$\left(8A_2I_{8_b}\right)$06 blade section with converging walls. The Mach numbers were obtained from measurements at static-pressure orifices at station A (fig. 1), since the attempt to measure Mach number from intersections of Mach waves (fig. 5) was unsatisfactory. The pressure loss, as well as the pressure rise, increases sharply between Mach number 0.9 and 1.0. The shock losses are probably responsible for the large increase in the loss coefficient. The pressure-rise parameter compares quite well with a point taken in a rotating machine near the same test conditions (ref. 5). Generally similar shock wave patterns are also shown in reference 5 for this blade section.

Some test results for the CW_1 blades are presented in figure 27 showing the combined effects of angle of attack and inlet angle change. The range of useful angle of attack is, as expected, rather small. At an angle of attack of 2°, β of 62°, it is apparent from the losses, pressure-rise coefficient and from the schlieren picture (fig. 10) that overexpansion has taken place on the upper surface creating a much higher Mach number; consequently, the steeper pressure rise through the

normal shock separates the flow near the trailing edge of the blade causing a normal shock in the passage and a higher pressure-loss coefficient.

Further test work was done on this blade section with the leading and trailing edges reversed. This configuration is designated CW_2 and test results at three values of α and β are shown in figure 28. A comparison of figure 28 with figure 27 at high Mach numbers shows that the sharp leading-edge profile CW_1 has lower losses and higher pressure rise than the blunt-nose profile CW_2.

An effort was made to determine the effect of inlet angle on the pressure-rise and pressure-loss coefficients using the CW_1 blade section. Figure 29 shows the pressure rises and losses for three angles of attack at inlet angles of 50°, 52°, and 54°. These values, when compared to those of figure 27 (high inlet angles), show an increase in loss coefficient. Decrease in performance is attributed to passage area approaching the upstream area; consequently, at the lower angles of attack a normal shock in the passage may cause severe separation.

A comparison is made in figure 30 of pressure-rise and pressure-loss coefficients plotted against Mach number for the blade sections CW_1 and 65-$(4A_{10})$06 at the optimum angle of attack. The pressure-loss coefficients are roughly the same, but the pressure rise for the wedge blade rises steeply through the Mach number range tested. The explanation, or a part of it, may be found in figures 14(b) and 14(c) and figures 20(b) and 20(c). In figure 14 the bow wave is attached; consequently, a strong normal shock is formed past the trailing edge of the upper surface and the pressure rise across this shock accounts for the favorable increase shown in figure 30. In figure 20 the bow wave would not attach to the thicker leading-edge section of the 65-series; consequently, a forked shock was formed on the upper surface and separation occurred, thereby decreasing the effective pressure rise.

CONCLUDING REMARKS

A transonic cascade has been designed and operated successfully by use of a variable-geometry nozzle and a slotted floor. Four compressor-blade configurations were tested over an inlet-angle range which is of interest to transonic and supersonic compressor designers. The results indicate that a transonic cascade is practical and will give results

applicable to compressor design. Cascade pressure rise is shown to be in fair agreement with the single-rotor test point which is available.

Langley Research Center,
National Aeronautics and Space Administration,
Langley Field, Va., August 28, 1959.

REFERENCES

1. Savage, Melvyn, and Felix, A. Richard: Investigation of a High-Performance Axial-Flow Compressor Transonic Inlet Rotor Designed for 37.5 Pounds Per Second Per Square Foot of Frontal Area - Aerodynamic Design and Overall Performance. NACA RM L55A05, 1955.

2. Kantrowitz, Arthur: The Supersonic Axial-Flow Compressor. NACA Rep. 974, 1950. (Supersedes NACA ACR L6D02.)

3. Dunavant, James C., Emery, James C., Walch, Howard C., and Westphal, Willard R.: High-Speed Cascade Tests of the NACA 65-$(12A_{10})10$ and NACA 65-$(12A_2I8_b)10$ Compressor Blade Sections. NACA RM L55I08, 1955.

4. Wright, Ray H., and Ward, Vernon G.: NACA Transonic Wind-Tunnel Test Sections. NACA Rep. 1231, 1955. (Supersedes NACA RM L8J06.)

5. Felix, A. Richard, and Savage, Melvyn: Investigation of a High-Performance Axial-Flow Compressor Transonic Inlet Rotor Designed for 37.5 Pounds Per Second Per Square Foot of Frontal Area - Detailed Blade-Element Performance. NACA RM L56K23, 1957.

TABLE I.- COORDINATES FOR T1-$(8A_2I8_b)$06 HAVING

6-PERCENT MAXIMUM THICKNESS

[Stations and ordinates in percent chord]

Percent chord	y	
	Upper surface	Lower surface
0		
.5	0.4582	-0.1904
.75	.5839	-.2039
1.25	.7875	-.1993
2.50	1.1850	-.1350
5.00	1.8321	.0161
7.50	2.3654	.1886
10.00	2.8375	.3604
15.00	3.6711	.6889
20.00	4.4082	.9679
25.00	5.0721	1.2096
30.00	5.6493	1.4246
35.00	6.1596	1.5964
40.00	6.5939	1.7404
45.00	6.9629	1.8311
50.00	7.2711	1.8611
55.00	7.5046	1.8293
60.00	7.6611	1.7329
65.00	7.6446	1.6454
70.00	7.4218	1.5821
75.00	6.9879	1.5143
80.00	6.3293	1.4064
85.00	5.3811	1.2532
90.00	4.1779	.9721
95.00	2.6539	.5161
100.00		
Leading-edge radius = 0.343 Trailing-edge radius = 1.000		

TABLE II.- COORDINATES FOR 65-$(4A_{10})$06 BLADE SECTION

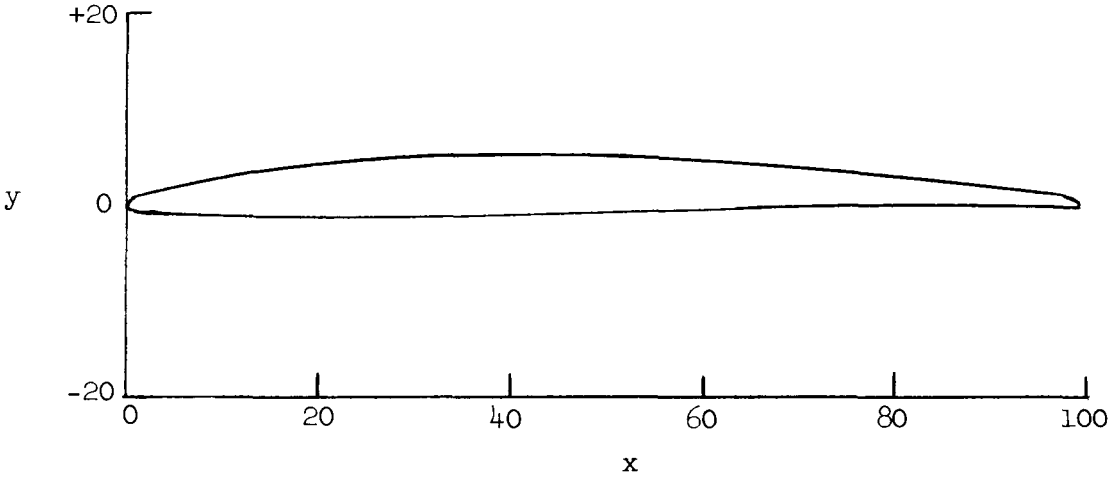

x	y_u	y_l
0	-----	------
1.25	0.924	-0.496
2.5	1.322	-.578
5.0	1.936	-.672
10	2.854	-.786
15	3.540	-.848
20	4.072	-.888
25	4.485	-.905
30	4.795	-.907
35	5.011	-.891
40	5.140	-.856
45	5.173	-.793
50	5.106	-.694
55	4.931	-.551
60	4.660	-.376
65	4.335	-.215
70	3.974	-.086
75	3.577	.003
80	3.136	.049
85	2.645	.047
90	2.089	-.021
95	1.443	-.179
100	-----	------

L. E. radius: 0.240	L. E. radius slope: 0.168
T. E. radius: 0.600	T. E. radius slope: 0.168

TABLE III.- BLADE TESTS

Blade section	σ	β, deg	α, deg	Figure
T1-$(8A_2I_{8_b})06$	0.80	56.1	13.6	5
CW_1	.80	58	-2	6, 7, 8
CW_1	.80	60	0	9
CW_1	.80	62	2	10
CW_2	.80	57	2	11
CW_2	.80	59	4	12
CW_2	.80	61	6	13
CW_1	.80	50	0	14
CW_1	.80	52	2	15, 16, 17
CW_1	.80	54	4	18, 19
65-$(4A_{10})06$	.80	50	2	20, 21
65-$(4A_{10})06$	.80	52	4	22, 23
65-$(4A_{10})06$	.80	54	6	24, 25

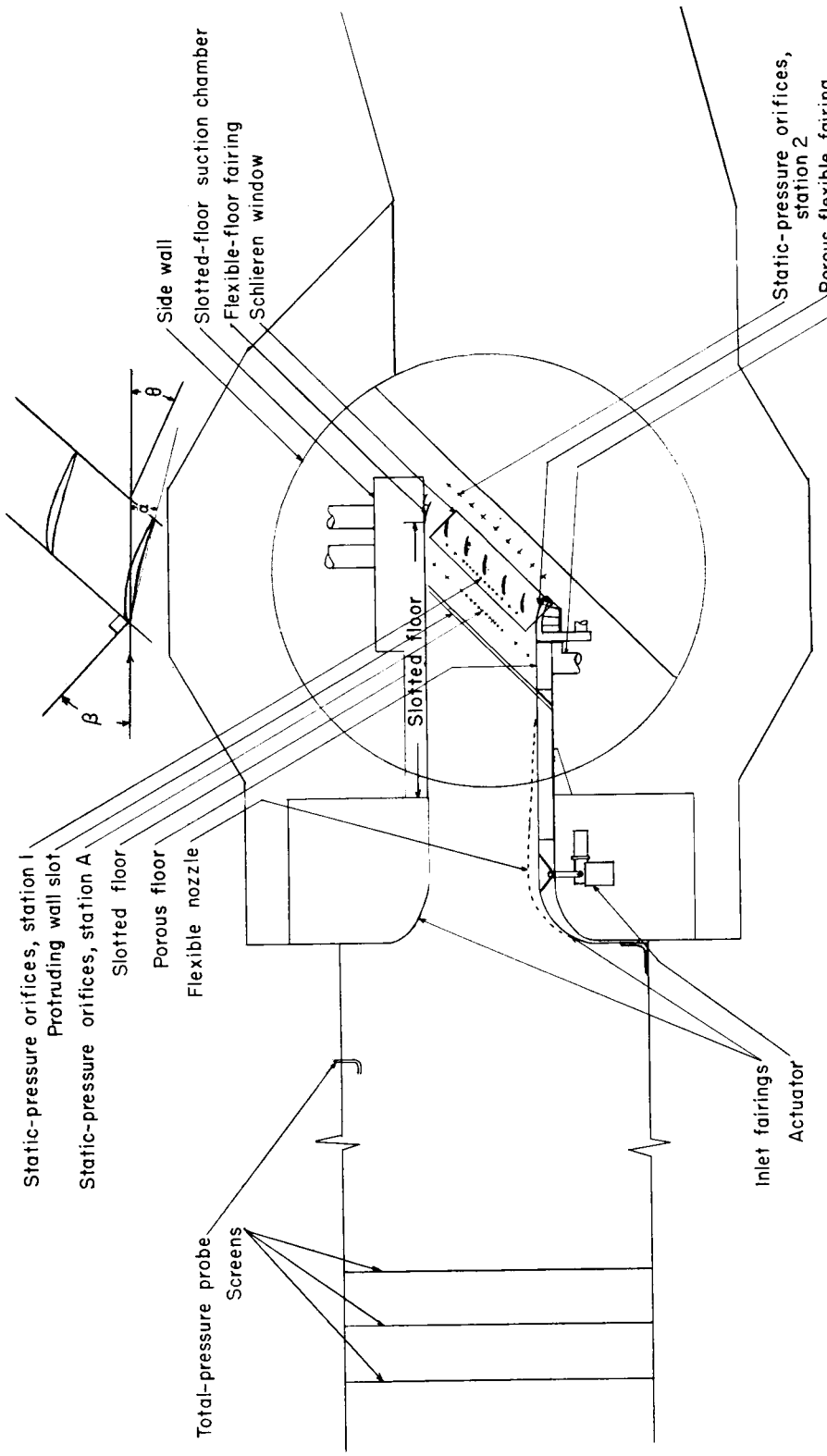

Figure 1.- Schematic cross-sectional view of a 7-inch transonic cascade tunnel.

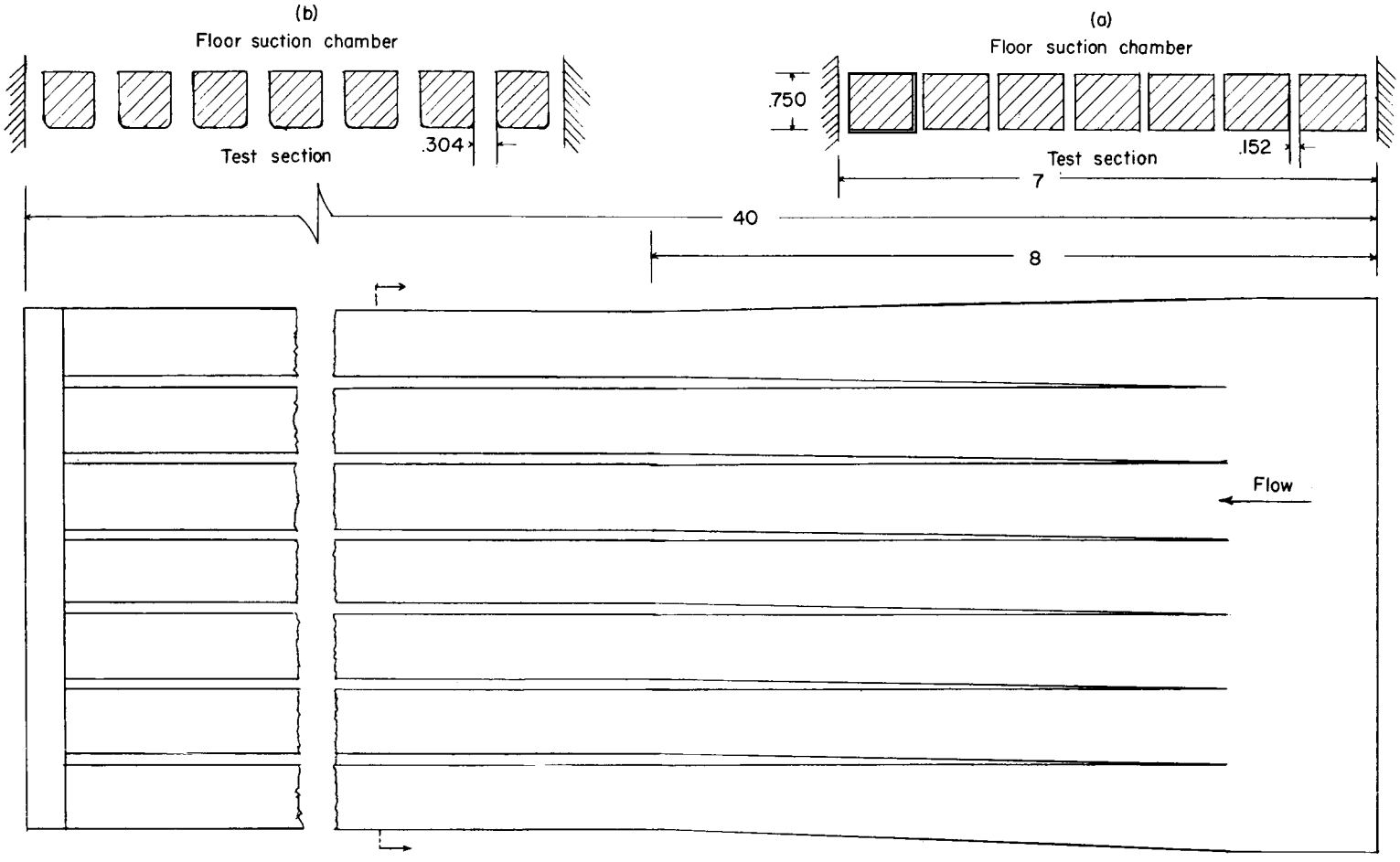

(a) Cross-sectional view, first design.

(b) Cross-sectional view, modified design.

Figure 2.- Upper floor slot design. (All dimensions are in inches.)

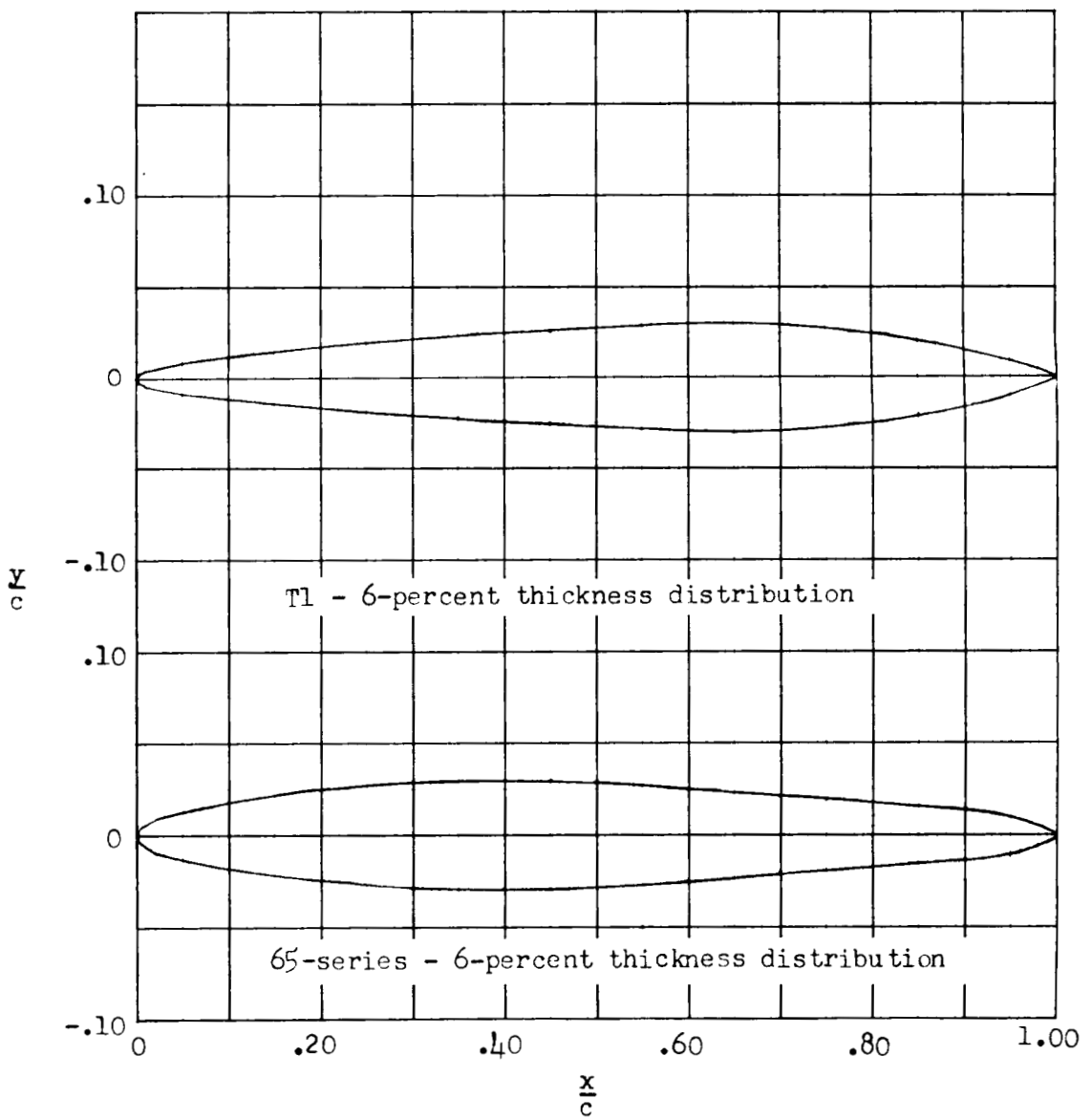

Figure 3.- Comparison of T1 and 65-series thickness distributions.

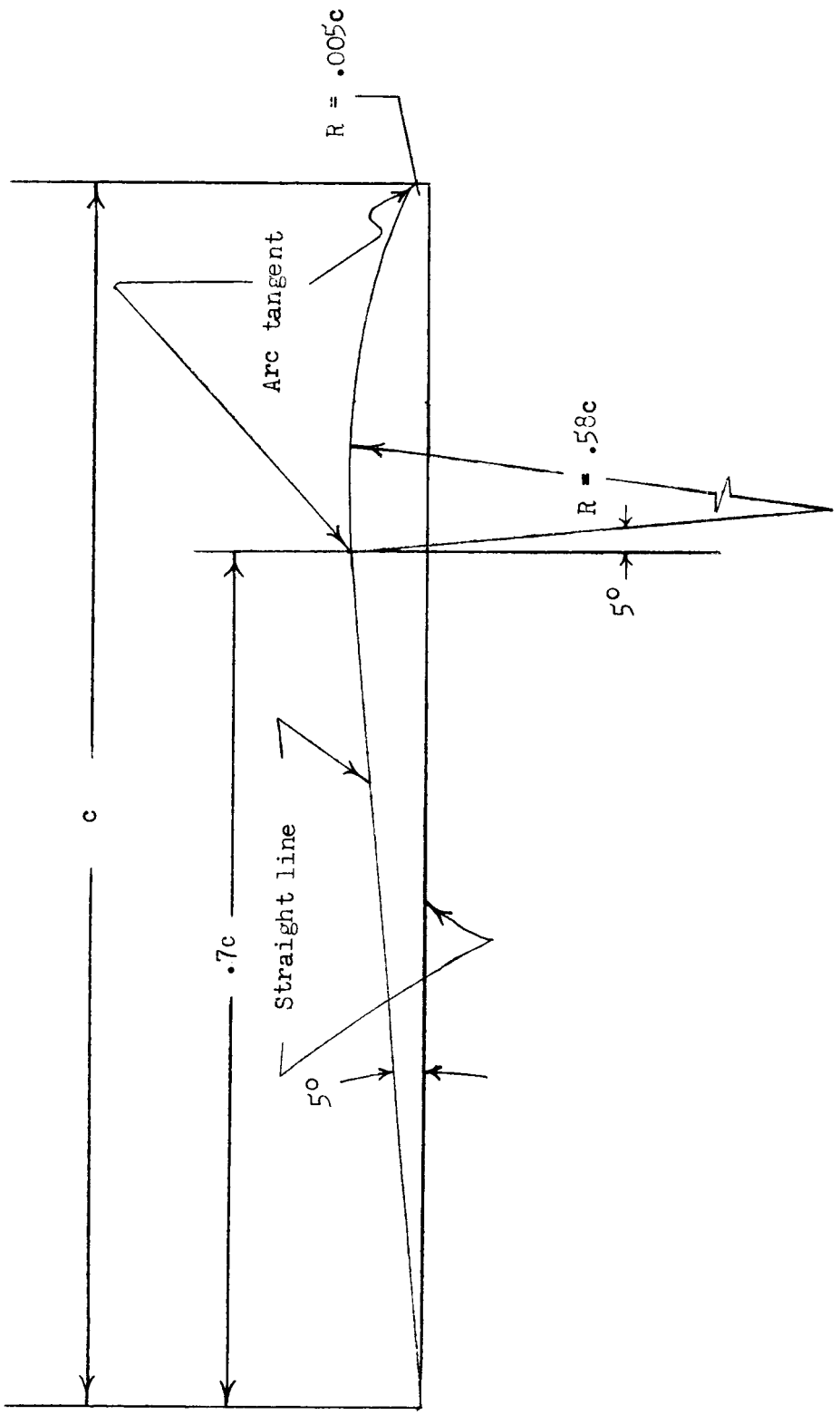

Figure 4.- Construction dimensions for the wedge circular-arc airfoil.

(a)

Station, percent c	M_b	
(a) $\bar{M}_1 = 1.03$		
80	0.819	Lower
60	.873	
50	.870	
40	.886	
30	.890	
20	.869	
10	.821	
5	1.456	Upper
10	1.426	
20	1.416	
30	1.451	
40	1.471	
50	1.512	
70	1.239	
90	1.248	

(b)

(b) $\bar{M}_1 = 1.08$		
80	0.754	Lower
60	.789	
50	.779	
40	.783	
30	.797	
20	.787	
10	.760	
5	1.446	Upper
10	1.412	
20	1.405	
30	1.441	
40	1.475	
50	1.526	
70	1.208	
90	1.214	

(c)

(c) $\bar{M}_1 = 1.14$		
80	0.827	Lower
60	.885	
50	.883	
40	.898	
30	.904	
20	.875	
10	.828	
5	1.450	Upper
10	1.421	
20	1.416	
30	1.435	
40	1.459	
50	1.505	
70	1.281	
90	1.283	

(d)

(d) $\bar{M}_1 = 1.18$		
80	0.843	Lower
60	.911	
50	.914	
40	.930	
30	.928	
20	.896	
10	.837	
5	1.498	Upper
10	1.490	
20	1.480	
30	1.528	
40	1.548	
50	1.542	
70	1.321	
90	1.317	

L-59-6043

Figure 5.- Schlieren photographs and Mach number distribution for tests of T1-$\left(8A_2I_{8_b}\right)$06 blade sections in converging-wall cascade at $\alpha = 13.6^\circ$, $\beta = 56.1^\circ$, and $\sigma = 0.80$.

(a)

Wall orifice	M_1	Station, percent c	M_b	
(a) $\frac{\Delta p_t}{q_1} = 0.0514$; $\bar{M}_1 = 1.227$; $\bar{M}_2 = 0.902$				
1	1.169	90	0.977	Lower
2	1.143	80	.950	
3	1.310	70	.926	
4	1.256	60	.912	
5	1.193	50	.910	
6	1.237	40	.917	
7	1.258	30	.923	
8	1.225	20	.900	
9	1.192	15	1.198	Upper
10	1.238	25	1.213	
11	1.230	35	1.222	
12	1.246	45	1.244	
13	1.254	55	1.292	
14	1.250	65	1.294	
15	1.246	75	1.446	
16	1.272	85	1.158	
17	-----	99	1.156	

(b)

(b) $\frac{\Delta p_t}{q_1} = 0.0637$; $\bar{M}_1 = 1.169$; $\bar{M}_2 = 0.901$				
1	1.108	90	0.956	Lower
2	1.178	80	.924	
3	1.170	70	.900	
4	1.270	60	.887	
5	1.221	50	.882	
6	1.273	40	.880	
7	1.288	30	.872	
8	1.224	20	.852	
9	1.088	15	1.289	Upper
10	1.188	25	1.291	
11	1.141	35	1.282	
12	1.096	45	1.292	
13	1.075	55	1.331	
14	1.040	65	1.515	
15	1.015	75	1.468	
16	1.030	85	1.188	
17	-----	99	1.188	

(c)

(c) $\frac{\Delta p_t}{q_1} = 0.0415$; $\bar{M}_1 = 1.144$; $\bar{M}_2 = 0.833$				
1	1.161	90	0.920	Lower
2	1.019	80	.888	
3	1.025	70	.863	
4	1.243	60	.858	
5	1.097	50	.854	
6	1.137	40	.853	
7	1.261	30	.852	
8	1.207	20	.840	
9	1.074	15	1.262	Upper
10	1.157	25	1.258	
11	1.226	35	1.261	
12	1.213	45	1.273	
13	1.178	55	1.312	
14	1.228	65	1.304	
15	1.246	75	1.034	
16	1.256	85	1.013	
17	-----	99	1.014	

(d)

(d) $\frac{\Delta p_t}{q_1} = 0.0512$; $\bar{M}_1 = 1.124$; $\bar{M}_2 = 0.835$				
1	1.121	90	0.908	Lower
2	1.043	80	.876	
3	1.017	70	.856	
4	1.251	60	.847	
5	1.097	50	.842	
6	1.150	40	.837	
7	1.297	30	.835	
8	1.210	20	.815	
9	1.044	15	1.268	Upper
10	1.157	25	1.254	
11	1.130	35	1.254	
12	1.086	45	1.265	
13	1.063	55	1.512	
14	1.069	65	1.512	
15	1.065	75	1.102	
16	1.087	85	1.051	
17	-----	99	1.057	

L-59-6044

Figure 6.- Schlieren photographs and Mach number distribution from cascade tests of CW_1 blade sections at $\alpha = -2^\circ$, $\beta = 58^\circ$, and $\sigma = 0.80$.

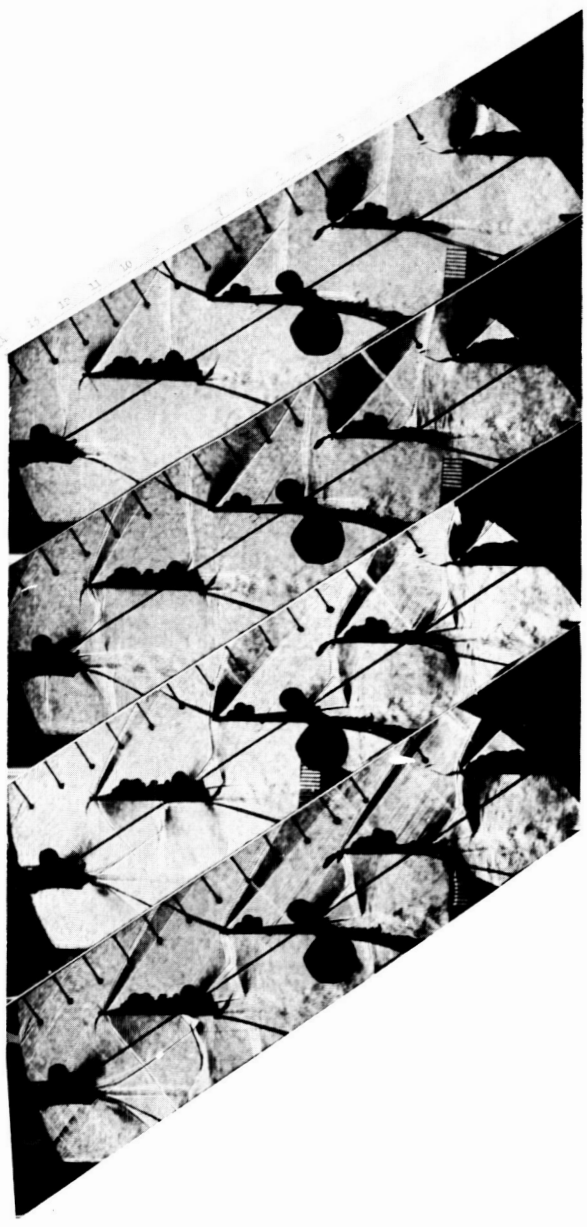

	Wall orifice	M_1	Station, percent c	M_b	
(a)	$\frac{\Delta p_t}{q_1} = 0.0176$; $\bar{M}_1 = 1.017$, $\bar{M}_2 = 0.723$				
	1	1.026	90	0.791	Lower
	2	.868	80	.768	
	3	.879	70	.752	
	4	1.072	60	.740	
	5	1.007	50	.739	
	6	.934	40	.736	
	7	1.163	30	.732	
	8	1.165	20	.718	
	9	.980	15	1.280	Upper
	10	.951	25	1.247	
	11	1.109	35	1.240	
	12	1.111	45	1.232	
	13	.990	55	1.260	
	14	.977	65	1.055	
	15	.983	75	.908	
	16	.958	85	.865	
	17	-----	95	.865	
(b)	$\frac{\Delta p_t}{q_1} = 0.0403$; $\bar{M}_1 = 1.107$, $\bar{M}_2 = 0.808$				
	1	1.056	90	0.891	Lower
	2	1.040	80	.857	
	3	1.004	70	.840	
	4	1.201	60	.829	
	5	1.038	50	.828	
	6	1.077	40	.826	
	7	1.140	30	.829	
	8	1.163	20	.821	
	9	1.014	15	1.172	Upper
	10	1.093	25	1.167	
	11	1.135	35	1.171	
	12	1.155	45	1.193	
	13	1.121	55	1.236	
	14	1.147	65	1.207	
	15	1.177	75	1.196	
	16	1.157	85	1.009	
	17	-----	95	1.006	
(c)	$\frac{\Delta p_t}{q_1} = 0.0537$; $\bar{M}_1 = 1.212$, $\bar{M}_2 = 0.902$				
	1	1.090	90	0.977	Lower
	2	1.177	80	.946	
	3	1.297	70	.923	
	4	1.226	60	.914	
	5	1.139	50	.908	
	6	1.260	40	.905	
	7	1.270	30	.892	
	8	1.212	20	.865	
	9	1.155	15	1.278	Upper
	10	1.245	25	1.269	
	11	1.236	35	1.252	
	12	1.225	45	1.204	
	13	1.242	55	1.237	
	14	1.220	65	1.220	
	15	1.224	75	1.178	
	16	1.256	85	1.162	
	17	-----	95	1.152	
(d)	$\frac{\Delta p_t}{q_1} = 0.0784$; $\bar{M}_1 = 1.266$, $\bar{M}_2 = 0.965$				
	1	1.122	90	0.989	Lower
	2	1.232	80	.963	
	3	1.340	70	.945	
	4	1.260	60	.939	
	5	1.316	50	.943	
	6	1.330	40	.947	
	7	1.313	30	.956	
	8	1.234	20	.892	
	9	1.232	15	1.380	Upper
	10	1.309	25	1.362	
	11	1.271	35	1.341	
	12	1.246	45	1.311	
	13	1.259	55	1.312	
	14	1.251	65	1.255	
	15	1.248	75	1.421	
	16	1.278	85	1.755	
	17	-----	95	1.466	

L-59-6045

Figure 7.- Schlieren photographs and Mach number distribution from cascade tests of CW_1 blade sections at $\alpha = -2^\circ$, $\beta = 58^\circ$, and $\sigma = 0.80$.

(a)

Wall orifice	M_1	Station percent c	M_b	
(a) $\frac{\Delta p_t}{q_1} = 0.0430$; $\bar{M}_1 = 1.119$, $\bar{M}_2 = 0.833$				
1	1.080	90	0.921	
2	1.056	80	.888	
3	1.038	70	.870	
4	1.208	60	.854	Lower
5	1.068	50	.852	
6	1.141	40	.846	
7	1.247	30	.842	
8	1.191	20	.824	
9	1.092	15	1.289	
10	1.134	25	1.269	
11	1.140	35	1.256	
12	1.114	45	1.249	
13	1.122	55	1.268	Upper
14	1.073	65	1.251	
15	1.014	75	1.115	
16	.962	85	1.025	
17	-----	99	1.025	

(b)

(b) $\frac{\Delta p_t}{q_1} = 0.0747$; $\bar{M}_1 = 1.248$, $\bar{M}_2 = 0.999$				
1	1.187	90	0.994	
2	1.325	80	.965	
3	1.315	70	.948	
4	1.296	60	.945	Lower
5	1.259	50	.942	
6	1.222	40	.935	
7	1.240	30	.929	
8	1.226	20	1.095	
9	1.226	15	1.185	
10	1.219	25	1.199	
11	1.237	35	1.230	
12	1.230	45	1.252	
13	1.240	55	1.287	Upper
14	1.239	65	1.281	
15	1.235	75	1.441	
16	1.253	85	1.762	
17	-----	99	1.764	

(c)

(c) $\frac{\Delta p_t}{q_1} = 0.0672$; $\bar{M}_1 = 1.38$, $\bar{M}_2 = 1.012$				
1	1.202	90	1.029	
2	1.371	80	1.009	
3	1.414	70	.990	
4	1.424	60	.986	
5	1.449	50	.996	Lower
6	1.415	40	.985	
7	1.396	30	.950	
8	1.392	20	.901	
9	1.433	15	1.469	
10	1.400	25	1.476	
11	1.365	35	1.458	
12	1.351	45	1.463	
13	1.345	55	1.485	Upper
14	1.342	65	1.447	
15	1.329	75	1.576	
16	1.358	85	1.390	
17	-----	99	1.582	

(d)

(d) $\frac{\Delta p_t}{q_1} = 0.0671$; $\bar{M}_1 = 1.39$, $\bar{M}_2 = 1.030$				
1	1.203	90	1.032	
2	1.456	80	1.014	
3	1.420	70	.999	
4	1.433	60	1.003	Lower
5	1.444	50	.999	
6	1.413	40	.966	
7	1.387	30	.937	
8	1.432	20	.990	
9	1.449	15	1.469	
10	1.403	25	1.478	
11	1.371	35	1.478	
12	1.360	45	1.470	
13	1.354	55	1.498	Upper
14	1.345	65	1.463	
15	1.342	75	1.599	
16	1.361	85	1.458	
17	-----	99	1.421	

L-59-6046

Figure 8.- Schlieren photographs and Mach number distribution from cascade tests of CW_1 blade sections at $\alpha = -2^\circ$, $\beta = 58^\circ$, and $\sigma = 0.80$.

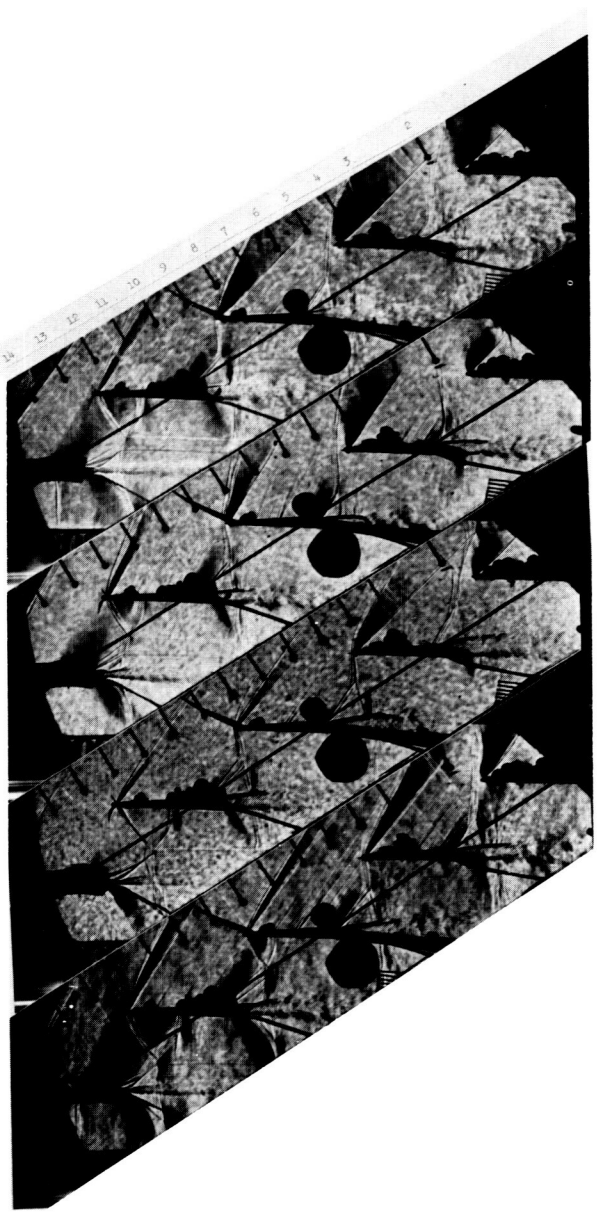

(a)

Wall orifice	M_1	Station, percent c	M_b	
(a) $\frac{\Delta p_t}{q_1} = 0.0428$; $\bar{M}_1 = 1.1965$; $\bar{M}_2 = 0.867$				
1	1.290	90	0.949	Lower
2	1.117	80	.917	
3	1.053	70	.900	
4	1.224	60	.892	
5	1.103	50	.894	
6	1.232	40	.894	
7	1.327	30	.886	
8	1.228	20	.853	
9	1.168	15	1.286	Upper
10	1.256	25	1.289	
11	1.220	35	1.305	
12	1.165	45	1.312	
13	1.162	55	1.334	
14	1.195	65	1.321	
15	1.213	75	1.122	
16	1.162	85	1.081	
17	-----	95	1.083	

(b)

(b) $\frac{\Delta p_t}{q_1} = 0.0387$; $\bar{M}_1 = 1.107$; $\bar{M}_2 = 0.863$				
1	1.128	90	0.958	Lower
2	1.051	80	.923	
3	1.038	70	.904	
4	1.121	60	.893	
5	1.047	50	.892	
6	1.068	40	.889	
7	1.092	30	.891	
8	1.098	20	.876	
9	1.108	15	1.117	Upper
10	1.148	25	1.072	
11	1.165	35	1.081	
12	1.149	45	1.093	
13	1.133	55	1.096	
14	1.123	65	1.108	
15	1.116	75	1.304	
16	1.132	85	1.066	
17	-----	95	1.075	

(c)

(c) $\frac{\Delta p_t}{q_1} = 0.0532$; $\bar{M}_1 = 1.295$; $\bar{M}_2 = 0.921$				
1	1.408	90	0.994	Lower
2	1.157	80	.973	
3	1.293	70	.959	
4	1.289	60	.943	
5	1.224	50	.939	
6	1.331	40	.927	
7	1.340	30	.903	
8	1.283	20	.894	
9	1.250	15	1.315	Upper
10	1.298	25	1.288	
11	1.319	35	1.259	
12	1.299	45	1.261	
13	1.312	55	1.290	
14	1.291	65	1.291	
15	1.283	75	1.480	
16	1.267	85	1.180	
17	-----	95	1.182	

(d)

(d) $\frac{\Delta p_t}{q_1} = 0.0455$; $\bar{M}_1 = 1.209$; $\bar{M}_2 = 0.920$				
1	1.228	90	0.998	Lower
2	1.202	80	.970	
3	1.217	70	.947	
4	1.231	60	.929	
5	1.193	50	.913	
6	1.243	40	.894	
7	1.250	30	.941	
8	1.242	20	1.217	Upper
9	1.220	15	1.219	
10	1.210	25	1.246	
11	1.242	35	1.261	
12	1.190	45	1.264	
13	1.146	55	1.273	
14	1.110	65	1.259	
15	1.135	75	1.426	
16	1.138	85	1.179	
17	-----	95	1.178	

L-59-6047

Figure 9.- Schlieren photographs and Mach number distribution from cascade tests of CW_1 blade sections at $\alpha = 0^\circ$, $\beta = 60^\circ$, and $\sigma = 0.80$.

	Wall orifice	M_1	Station percent c	M_b	
(a)	$\frac{\Delta p_t}{q_1} = 0.0913$; $\bar{M}_1 = 1.267$, $\bar{M}_2 = 0.886$				
	1	-----	90	0.958	
	2	-----	80	.926	
	3	1.087	70	.911	
	4	1.329	60	.914	Lower
	5	1.156	50	.931	
	6	1.115	40	.944	
	7	1.240	30	.943	
	8	1.301	20	.890	
	9	1.211	15	1.425	
	10	1.407	25	1.431	
	11	1.397	35	1.449	
	12	1.299	45	1.385	Upper
	13	1.255	55	1.142	
	14	1.349	65	1.112	
	15	1.341	75	1.102	
	16	1.267	85	1.097	
(b)	17	-----	95	1.099	
	(b) $\frac{\Delta p_t}{q_1} = 0.0847$; $\bar{M}_1 = 1.374$, $\bar{M}_2 = 0.948$				
	1	-----	90	1.005	
	2	-----	80	.980	
	3	1.157	70	.963	
	4	1.287	60	.961	Lower
	5	1.251	50	1.018	
	6	1.241	40	1.065	
	7	1.372	30	1.022	
	8	1.407	20	.926	
	9	1.431	15	1.554	
	10	1.483	25	1.543	
(c)	11	1.450	35	1.512	
	12	1.426	45	1.492	Upper
	13	1.469	55	1.485	
	14	1.477	65	1.414	
	15	1.415	75	1.193	
	16	1.426	85	1.173	
	17	-----	95	1.175	
	(c) $\frac{\Delta p_t}{q_1} = 0.0865$; $\bar{M}_1 = 1.384$, $\bar{M}_2 = 0.950$				
	1	-----	90	1.008	
	2	-----	80	.980	
	3	1.171	70	.964	
	4	1.298	60	.963	Lower
	5	1.276	50	1.007	
	6	1.255	40	1.050	
(d)	7	1.432	30	1.003	
	8	1.417	20	.916	
	9	1.440	15	1.567	
	10	1.480	25	1.550	
	11	1.445	35	1.536	
	12	1.425	45	1.518	Upper
	13	1.468	55	1.483	
	14	1.473	65	1.437	
	15	1.398	75	1.184	
	16	1.405	85	1.169	
	17	-----	95	1.170	
	(d) $\frac{\Delta p_t}{q_1} = 0.0768$; $\bar{M}_1 = 1.380$, $\bar{M}_2 = 0.959$				
	1	-----	90	1.005	
	2	-----	80	.976	
	3	1.233	70	.965	
	4	1.339	60	.968	
	5	1.250	50	1.001	Lower
	6	1.440	40	1.023	
	7	1.445	30	.980	
	8	1.403	20	.903	
	9	1.405	15	1.493	
	10	1.426	25	1.477	
	11	1.425	35	1.450	
	12	1.374	45	1.456	
	13	1.402	55	1.415	Upper
	14	1.428	65	1.382	
	15	1.371	75	1.252	
	16	1.317	85	1.168	
	17	-----	95	1.172	

L-59-6048

Figure 10.- Schlieren photographs and Mach number distribution from cascade tests of CW_1 blade sections at $\alpha = 2^\circ$, $\beta = 62^\circ$, and $\sigma = 0.80$.

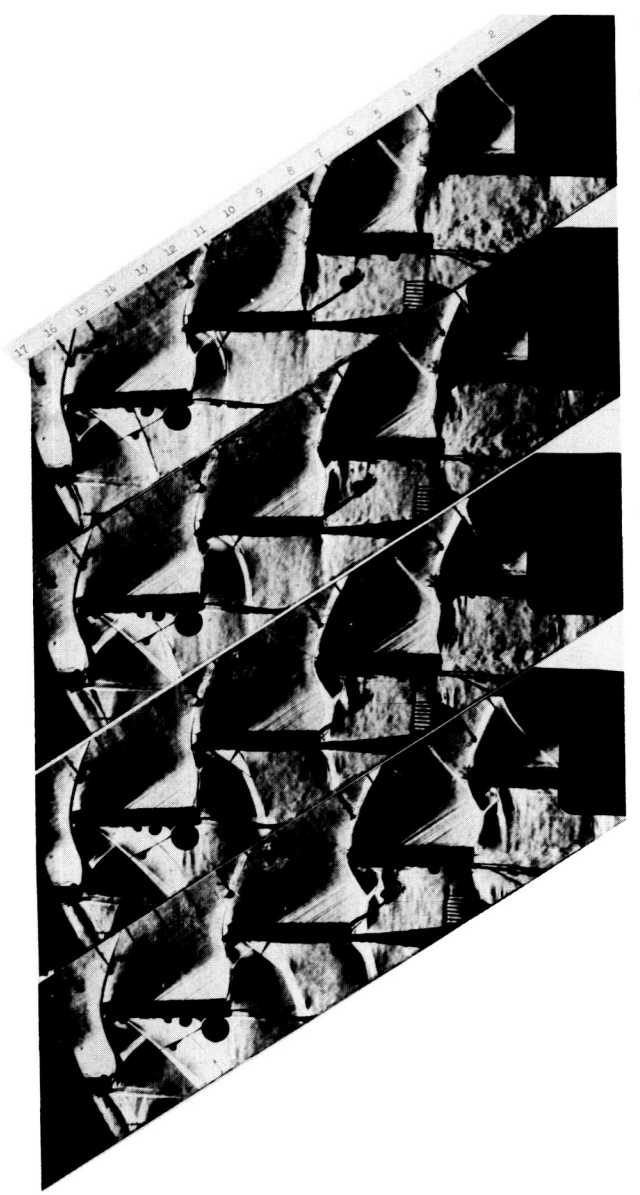

(a)

Wall orifice	M_1	Station percent c	M_b	
(a) $\frac{\Delta p_t}{q_1} = 0.0958$; $\bar{M}_1 = 1.12$, $\bar{M}_2 = 0.930$				
1	-----	80	0.988	Lower
2	-----	70	.966	
3	1.133	60	.956	
4	1.065	50	.946	
5	1.268	40	.976	
6	1.223	30	1.084	
7	1.138	20	1.233	
8	.986	10	1.671	
9	1.066	5	.813	
10	1.231	15	1.166	Upper
11	1.136	25	1.494	
12	1.103	35	1.623	
13	1.243	45	1.590	
14	1.154	55	1.607	
15	1.053	65	1.539	
16	.992	75	1.302	
17	1.211	85	1.188	

(b)

(b) $\frac{\Delta p_t}{q_1} = 0.0925$; $\bar{M}_1 = 1.137$, $\bar{M}_2 = 0.961$				
1	-----	80	1.000	Lower
2	-----	70	.972	
3	1.144	60	.960	
4	1.100	50	.956	
5	1.289	40	1.025	
6	1.230	30	1.160	
7	1.142	20	1.402	
8	.956	10	1.671	
9	1.056	5	.796	
10	1.238	15	1.153	Upper
11	1.130	25	1.484	
12	1.086	35	1.611	
13	1.235	45	1.573	
14	1.149	55	1.597	
15	1.060	65	1.596	
16	1.001	75	1.541	
17	1.208	85	1.478	

(c)

(c) $\frac{\Delta p_t}{q_1} = 0.0829$; $\bar{M}_1 = 1.145$, $\bar{M}_2 = 0.990$				
1	-----	80	1.008	Lower
2	-----	70	.978	
3	1.158	60	.966	
4	1.137	50	.974	
5	1.298	40	1.057	
6	1.241	30	1.221	
7	1.144	20	1.625	
8	.984	10	1.699	
9	1.117	5	.784	
10	1.241	15	1.145	Upper
11	1.121	25	1.465	
12	1.063	35	1.587	
13	1.228	45	1.546	
14	1.145	55	1.577	
15	1.068	65	1.578	
16	1.019	75	1.581	
17	1.219	85	1.597	

(d)

(d) $\frac{\Delta p_t}{q_1} = 0.0709$; $\bar{M}_1 = 1.155$, $\bar{M}_2 = 1.023$				
1	-----	80	1.012	Lower
2	-----	70	.992	
3	1.161	60	.990	
4	1.163	50	1.027	
5	1.299	40	1.153	
6	1.243	30	1.487	
7	1.147	20	1.641	
8	1.016	10	1.707	
9	1.148	5	.779	
10	1.240	15	1.141	Upper
11	1.118	25	1.463	
12	1.054	35	1.585	
13	1.228	45	1.506	
14	1.153	55	1.575	
15	1.089	65	1.575	
16	1.033	75	1.582	
17	1.229	85	1.593	

L-59-6049

Figure 11.- Schlieren photographs and Mach number distribution from cascade tests of CW_2 blade sections at $\alpha = 2^\circ$, $\beta = 57^\circ$, and $\sigma = 0.80$.

(a)

(a) $\frac{\Delta p_t}{q_1} = 0.0799$; $\bar{M}_1 = 1.130$; $\bar{M}_2 = 0.869$

Wall orifice	M_1	Station, percent c	M_b	
1	-----	80	0.942	Lower
2	-----	70	.939	
3	1.111	60	.939	
4	1.021	50	.931	
5	1.094	40	.934	
6	1.106	30	.929	
7	1.093	20	.919	
8	-----	10	1.004	
9	-----	5	.821	
10	1.150	15	1.158	Upper
11	1.138	25	1.479	
12	1.055	35	1.443	
13	1.172	45	1.290	
14	1.212	55	1.209	
15	1.136	65	1.167	
16	1.079	75	1.076	
17	1.231	85	1.045	

(b)

(b) $\frac{\Delta p_t}{q_1} = 0.1081$; $\bar{M}_1 = 1.196$; $\bar{M}_2 = 0.970$

1	-----	80	1.014	Lower
2	-----	70	.990	
3	1.181	60	.995	
4	1.171	50	1.020	
5	1.322	40	1.116	
6	1.258	30	1.221	
7	1.172	20	1.359	
8	-----	10	1.707	
9	-----	5	.809	
10	1.245	15	1.155	Upper
11	1.129	25	1.467	
12	1.058	35	1.600	
13	1.278	45	1.525	
14	1.202	55	1.596	
15	1.122	65	1.599	
16	1.100	75	1.539	
17	1.267	85	1.349	

(c)

(c) $\frac{\Delta p_t}{q_1} = 0.1015$; $\bar{M}_1 = 1.214$; $\bar{M}_2 = 1.001$

1	-----	80	1.030	Lower
2	-----	70	1.006	
3	1.208	60	1.021	
4	1.228	50	1.074	
5	1.325	40	1.163	
6	1.262	30	1.261	
7	1.192	20	1.482	
8	-----	10	1.700	
9	-----	5	.851	
10	1.256	15	1.189	Upper
11	1.124	25	1.517	
12	1.139	35	1.623	
13	1.289	45	1.483	
14	1.224	55	1.561	
15	1.136	65	1.556	
16	1.129	75	1.556	
17	1.286	85	1.543	

(d)

(d) $\frac{\Delta p_t}{q_1} = 0.0988$; $\bar{M}_1 = 1.217$; $\bar{M}_2 = 1.003$

1	-----	80	1.030	Lower
2	-----	70	1.003	
3	1.213	60	1.014	
4	1.232	50	1.061	
5	1.327	40	1.150	
6	1.262	30	1.251	
7	1.192	20	1.504	
8	-----	10	1.690	
9	-----	5	.852	
10	1.233	15	1.186	Upper
11	1.120	25	1.512	
12	1.155	35	1.627	
13	1.292	45	1.507	
14	1.222	55	1.564	
15	1.140	65	1.547	
16	1.138	75	1.551	
17	1.290	85	1.551	

L-59-6050

Figure 12.- Schlieren photographs and Mach number distribution from cascade tests of CW_2 blade sections at $\alpha = 4^\circ$, $\beta = 59^\circ$, and $\sigma = 0.80$.

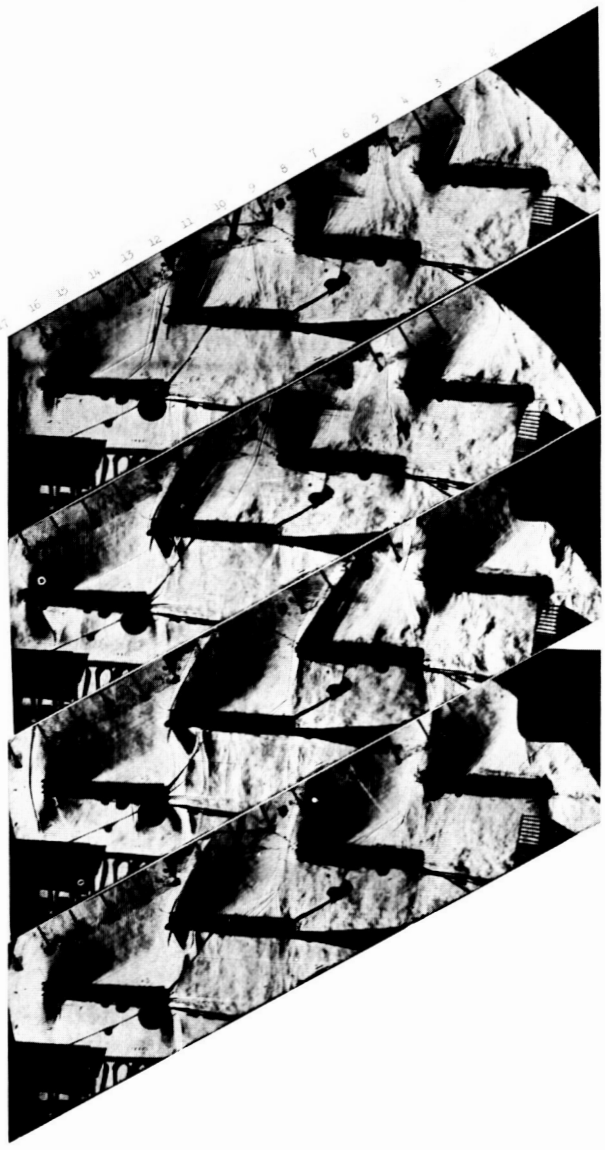

(a)

Wall orifice	M_1	Station, percent c	M_b	
(a) $\frac{\Delta p_t}{q_1} = 0.1367$; $\bar{M}_1 = 1.117$; $\bar{M}_2 = 0.847$				
1	1.187	80	0.943	Lower
2	.984	70	.929	
3	1.109	60	.932	
4	1.057	50	.916	
5	.995	40	.921	
6	1.083	30	.910	
7	1.172	20	.894	
8	-----	10	.880	
9	-----	5	.959	
10	1.102	15	1.262	Upper
11	1.149	25	1.190	
12	1.093	35	1.124	
13	1.251	45	1.122	
14	1.215	55	1.127	
15	1.118	65	1.129	
16	-----	75	1.106	
17	-----	85	1.106	

(b)

(b) $\frac{\Delta p_t}{q_1} = 0.0896$; $\bar{M}_1 = 1.195$; $\bar{M}_2 = 0.916$				
1	1.338	80	0.989	Lower
2	1.067	70	.960	
3	1.212	60	.951	
4	1.074	50	.958	
5	1.059	40	1.007	
6	1.219	30	1.094	
7	1.191	20	1.187	
8	-----	10	1.447	
9	-----	5	.912	
10	1.311	15	1.249	Upper
11	1.200	25	1.347	
12	1.229	35	1.250	
13	1.310	45	1.209	
14	1.214	55	1.192	
15	1.116	65	1.194	
16	-----	75	1.185	
17	-----	85	1.185	

(c)

(c) $\frac{\Delta p_t}{q_1} = 0.1436$; $\bar{M}_1 = 1.241$; $\bar{M}_2 = 0.969$				
1	1.452	80	1.002	Lower
2	1.386	70	.984	
3	1.183	60	.998	
4	1.070	50	1.053	
5	1.134	40	1.139	
6	1.311	30	1.251	
7	1.289	20	1.297	
8	-----	10	1.447	
9	-----	5	.905	
10	1.269	15	1.240	Upper
11	1.170	25	1.561	
12	1.195	35	1.685	
13	1.292	45	1.606	
14	1.235	55	1.632	
15	1.153	65	1.587	
16	-----	75	1.486	
17	-----	85	1.340	

(d)

(d) $\frac{\Delta p_t}{q_1} = 0.1002$; $\bar{M}_1 = 1.199$; $\bar{M}_2 = 0.926$				
1	1.220	80	0.987	Lower
2	1.109	70	.963	
3	1.216	60	.971	
4	1.110	50	.968	
5	1.167	40	1.004	
6	1.274	30	1.070	
7	1.178	20	1.164	
8	-----	10	1.351	
9	-----	5	.899	
10	1.286	15	1.258	Upper
11	1.197	25	1.548	
12	1.182	35	1.633	
13	1.310	45	1.528	
14	1.217	55	1.477	
15	1.116	65	1.246	
16	-----	75	1.202	
17	-----	85	1.152	

L-59-6051

Figure 13.- Schlieren photographs and Mach number distribution from cascade tests of CW_2 blade sections at $\alpha = 6^\circ$, $\beta = 61^\circ$, and $\sigma = 0.80$.

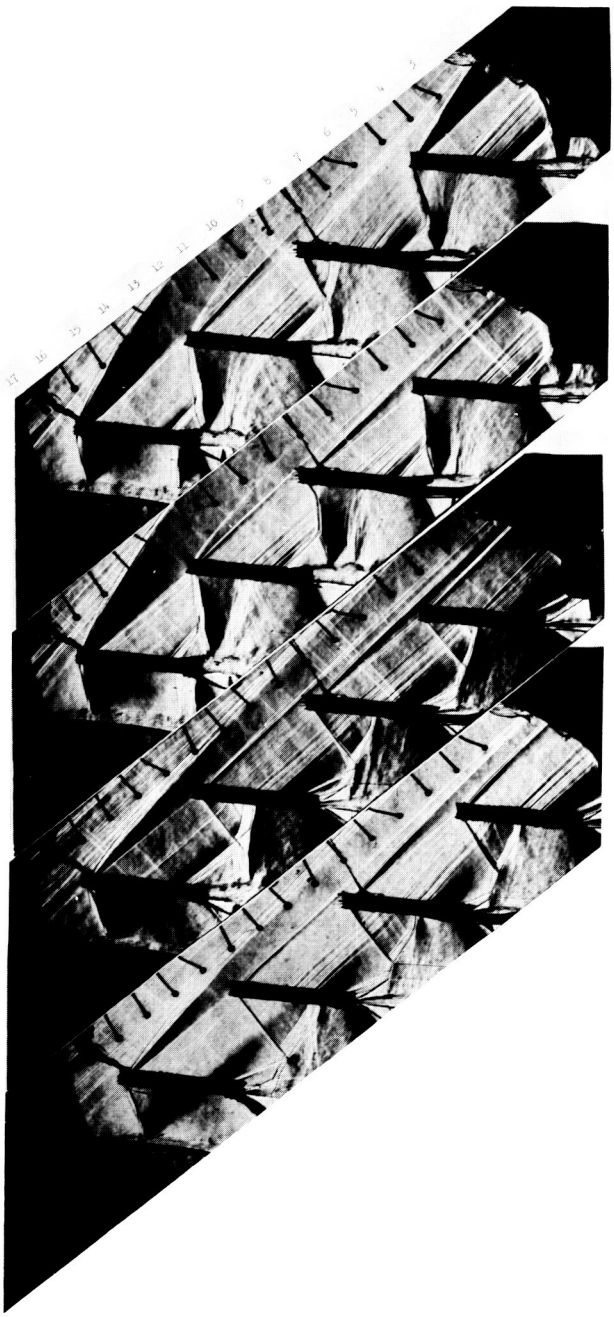

	Wall orifice	M_1	Station, percent c	M_b	
(a)	(a) $\frac{\Delta p_t}{q_1} = 0.0502$; $\bar{M}_1 = 1.267$, $\bar{M}_2 = 0.964$				
	1	0.959	90	0.990	Lower
	2	1.297	80	.965	
	3	1.296	70	.952	
	4	1.268	60	.937	
	5	1.355	50	.921	
	6	1.345	40	.904	
	7	1.280	30	1.059	
	8	1.224	20	1.167	
	9	1.300	15	1.229	Upper
	10	1.287	25	1.248	
	11	1.272	35	1.259	
	12	1.279	45	1.251	
	13	1.301	55	1.194	
	14	1.276	65	1.257	
(b)	15	-----	75	1.422	
	16	-----	85	1.245	
	17	-----	95	1.251	
(b)	(b) $\frac{\Delta p_t}{q_1} = 0.0612$; $\bar{M}_1 = 1.330$, $\bar{M}_2 = 0.964$				
	1	0.962	90	0.999	Lower
	2	1.419	80	.979	
	3	1.407	70	.967	
	4	1.402	60	.964	
	5	1.378	50	.960	
	6	1.323	40	.927	
	7	1.363	30	.892	
	8	1.368	20	.864	
	9	1.366	15	1.478	Upper
	10	1.307	25	1.470	
	11	1.354	35	1.458	
	12	1.349	45	1.421	
	13	1.322	55	1.404	
	14	1.306	65	1.301	
(c)	15	-----	75	1.460	
	16	-----	85	1.209	
	17	-----	95	1.201	
(c)	(c) $\frac{\Delta p_t}{q_1} = 0.0604$; $\bar{M}_1 = 1.399$, $\bar{M}_2 = 1.017$				
	1	1.011	90	1.013	Lower
	2	1.401	80	.981	
	3	1.435	70	.947	
	4	1.399	60	.905	
	5	1.376	50	.886	
	6	1.342	40	1.137	
	7	1.391	30	1.274	
	8	1.406	20	1.259	
	9	1.356	15	1.484	Upper
	10	1.399	25	1.509	
	11	1.407	35	1.506	
	12	1.384	45	1.481	
(d)	13	-----	55	1.445	
	14	-----	65	1.456	
	15	-----	75	1.544	
	16	-----	85	1.414	
	17	1.452	95	1.366	
(d)	(d) $\frac{\Delta p_t}{q_1} = 0.0790$; $\bar{M}_1 = 1.353$, $\bar{M}_2 = 1.068$				
	1	1.054	90	0.986	Lower
	2	1.346	80	.940	
	3	1.410	70	.954	
	4	1.400	60	1.178	
	5	1.397	50	1.263	
	6	1.324	40	1.220	
	7	1.371	30	1.238	
	8	1.378	20	1.228	
	9	1.360	15	1.445	Upper
	10	1.389	25	1.418	
	11	1.409	35	1.347	
	12	1.405	45	1.324	
	13	-----	55	1.289	
	14	-----	65	1.296	
	15	-----	75	1.486	
	16	-----	85	1.802	
	17	-----	95	1.612	

L-59-6052

Figure 14.- Schlieren photographs and Mach number distribution from cascade tests of CW_1 blade sections at $\alpha = 0^\circ$, $\beta = 50^\circ$, and $\sigma = 0.80$.

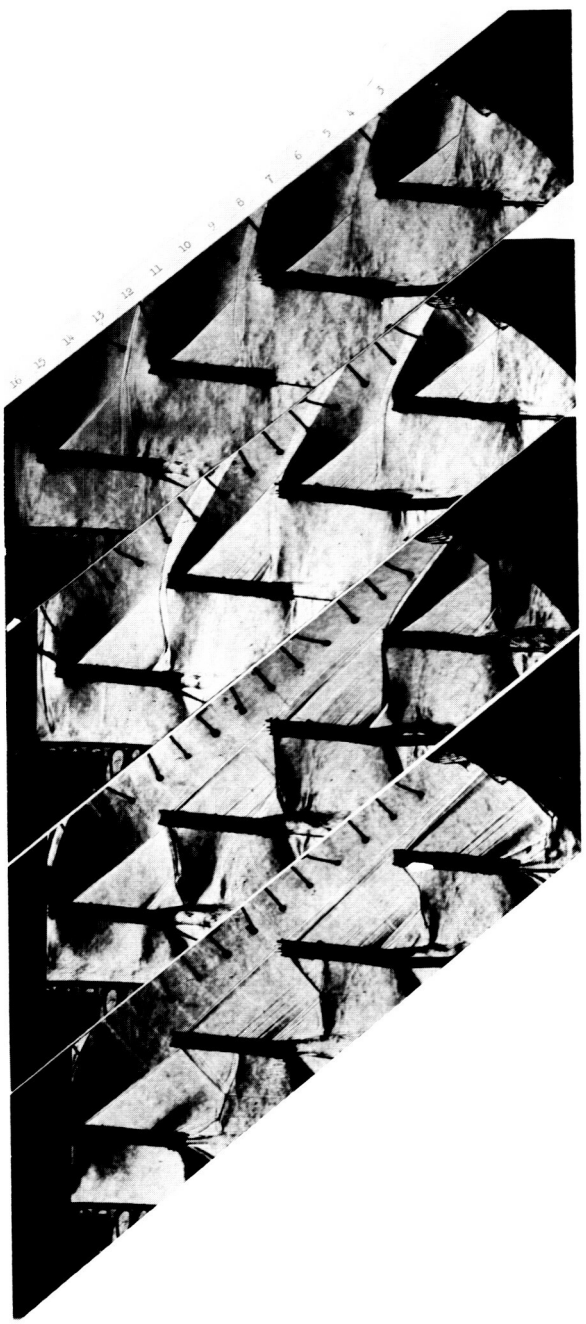

(a)

Wall orifice	M_1	Station, percent c	M_b	
(a) $\frac{\Delta p_t}{q_1} = 0.0610$; $\bar{M}_1 = 1.075$, $\bar{M}_2 = 0.828$				
1	0.818	90	0.904	Lower
2	1.070	80	.878	
3	1.158	70	.861	
4	1.056	60	.847	
5	1.054	50	.842	
6	1.217	40	.839	
7	1.133	30	.818	
8	1.055	20	.787	
9	1.054	15	1.374	Upper
10	1.162	25	1.331	
11	1.127	35	1.324	
12	1.065	45	1.321	
13	1.054	55	1.319	
14	1.062	65	1.086	
15	1.067	75	.959	
16	1.041	85	.979	
17	-----	95	.979	

(b)

(b) $\frac{\Delta p_t}{q_1} = 0.0661$; $\bar{M}_1 = 1.188$, $\bar{M}_2 = 0.880$				
1	0.866	90	0.954	Lower
2	1.213	80	.925	
3	1.210	70	.911	
4	1.195	60	.901	
5	1.292	50	.895	
6	1.250	40	.898	
7	1.212	30	.879	
8	1.207	20	.842	
9	1.290	15	1.421	Upper
10	1.230	25	1.403	
11	1.185	35	1.392	
12	1.163	45	1.388	
13	1.171	55	1.383	
14	1.192	65	1.369	
15	1.177	75	1.072	
16	1.145	85	1.064	
17	-----	95	1.065	

(c)

(c) $\frac{\Delta p_t}{q_1} = 0.0701$; $\bar{M}_1 = 1.301$, $\bar{M}_2 = 0.941$				
1	0.951	90	0.993	Lower
2	1.330	80	.966	
3	1.402	70	.954	
4	1.399	60	.949	
5	1.420	50	.946	
6	1.404	40	.938	
7	1.385	30	.913	
8	1.331	20	.873	
9	1.359	15	1.418	Upper
10	1.339	25	1.391	
11	1.326	35	1.320	
12	1.303	45	1.294	
13	1.282	55	1.279	
14	1.249	65	1.327	
15	1.197	75	1.503	
16	1.173	85	1.175	
17	-----	95	1.175	

(d)

(d) $\frac{\Delta p_t}{q_1} = 0.0665$; $\bar{M}_1 = 1.338$, $\bar{M}_2 = 1.018$				
1	1.009	90	1.017	Lower
2	1.425	80	.986	
3	1.489	70	.967	
4	1.418	60	.952	
5	1.427	50	.896	
6	1.398	40	.879	
7	1.343	30	1.097	
8	1.403	20	1.275	
9	1.585	15	1.394	Upper
10	1.560	25	1.431	
11	1.555	35	1.428	
12	1.551	45	1.458	
13	1.517	55	1.440	
14	1.281	65	1.455	
15	1.231	75	1.542	
16	1.216	85	1.319	
17	-----	95	1.316	

L-59-6053

Figure 15.- Schlieren photographs and Mach number distribution from cascade tests of CW_1 blade sections at $\alpha = 2^\circ$, $\beta = 52^\circ$, and $\sigma = 0.80$.

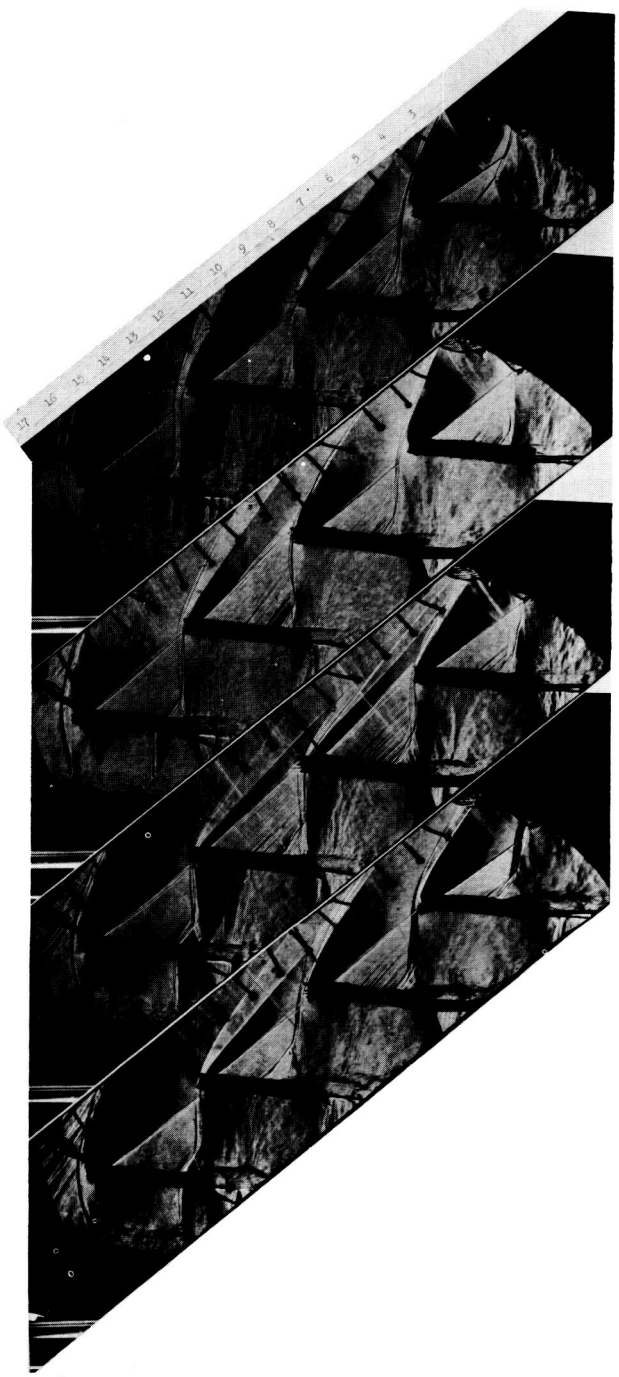

(a)

Wall orifice	M_1	Station, percent c	M_2	
(a) $\frac{\Delta p_t}{q_1} = 0.0705$; $\bar{M}_1 = 1.193$; $\bar{M}_2 = 0.876$				
1	0.869	90	0.963	Lower
2	1.182	80	.931	
3	1.196	70	.915	
4	1.169	60	.902	
5	1.312	50	.895	
6	1.288	40	.897	
7	1.272	30	.879	
8	1.259	20	.847	
9	1.256	15	1.382	Upper
10	1.197	25	1.382	
11	1.152	35	1.393	
12	1.183	45	1.403	
13	1.229	55	1.411	
14	1.217	65	1.230	
15	1.182	75	1.088	
16	1.132	85	1.088	
17	-----	95	1.084	

(b)

(b) $\frac{\Delta p_t}{q_1} = 0.0639$; $\bar{M}_1 = 1.193$; $\bar{M}_2 = 0.880$				
1	0.867	90	0.955	Lower
2	1.198	80	.924	
3	1.200	70	.909	
4	1.157	60	.896	
5	1.286	50	.888	
6	1.299	40	.892	
7	1.258	30	.876	
8	1.269	20	.845	
9	1.287	15	1.442	Upper
10	1.206	25	1.429	
11	1.149	35	1.419	
12	1.181	45	1.382	
13	1.222	55	1.349	
14	1.198	65	1.334	
15	1.166	75	1.099	
16	1.145	85	1.082	
17	-----	95	1.083	

(c)

(c) $\frac{\Delta p_t}{q_1} = 0.0671$; $\bar{M}_1 = 1.246$; $\bar{M}_2 = 0.906$				
1	0.894	90	0.973	Lower
2	1.259	80	.944	
3	1.245	70	.931	
4	1.304	60	.919	
5	1.379	50	.913	
6	1.343	40	.918	
7	1.369	30	.903	
8	1.289	20	.871	
9	1.265	15	1.526	Upper
10	1.240	25	1.532	
11	1.244	35	1.545	
12	1.257	45	1.565	
13	1.256	55	1.580	
14	1.225	65	1.430	
15	1.193	75	1.158	
16	1.182	85	1.118	
17	-----	95	1.121	

(d)

(d) $\frac{\Delta p_t}{q_1} = 0.0707$; $\bar{M}_1 = 1.243$; $\bar{M}_2 = 0.907$				
1	0.900	90	0.979	Lower
2	1.297	80	.950	
3	1.258	70	.941	
4	1.279	60	.932	
5	1.324	50	.931	
6	1.339	40	.933	
7	1.258	30	.910	
8	1.217	20	.867	
9	1.292	15	1.589	Upper
10	1.273	25	1.562	
11	1.256	35	1.523	
12	1.271	45	1.515	
13	1.288	55	1.515	
14	1.256	65	1.340	
15	1.203	75	1.181	
16	1.173	85	1.107	
17	-----	95	1.107	

L-59-6054

Figure 16.- Schlieren photographs and Mach number distribution from cascade tests of CW_1 blade sections at $\alpha = 2^\circ$, $\beta = 52^\circ$, and $\sigma = 0.80$.

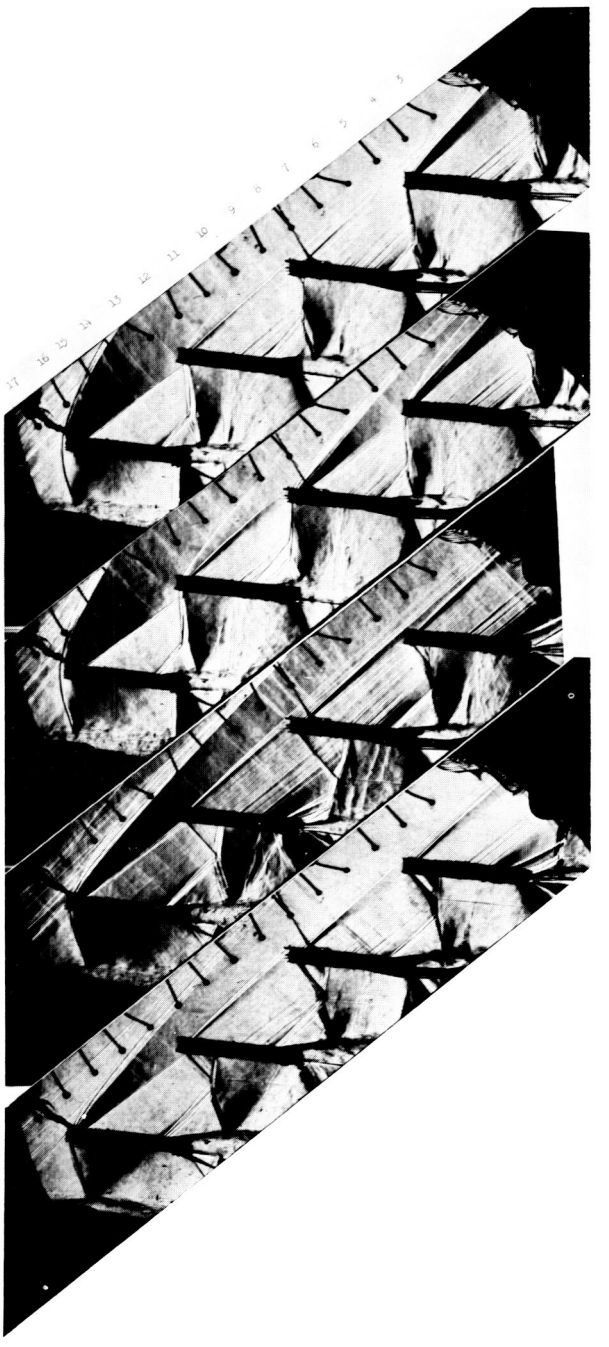

(a)

Wall orifice	M_1	Station, percent c	M_b	
(a) $\frac{\Delta p_t}{q_1} = 0.0669$; $\bar{M}_1 = 1.322$, $\bar{M}_2 = 0.969$				
1	0.962	90	1.006	Lower
2	1.383	80	.982	
3	1.413	70	.976	
4	1.363	60	.976	
5	1.437	50	.979	
6	1.414	40	.958	
7	1.335	30	.922	
8	1.318	20	.868	
9	1.359	15	1.382	Upper
10	1.325	25	1.404	
11	1.328	35	1.409	
12	1.342	45	1.402	
13	1.321	55	1.363	
14	1.284	65	1.390	
15	1.240	75	1.322	
16	-----	85	1.215	
17	-----	95	1.219	

(b)

Wall orifice	M_1	Station, percent c	M_b	
(b) $\frac{\Delta p_t}{q_1} = 0.0938$; $\bar{M}_1 = 1.334$, $\bar{M}_2 = 0.968$				
1	0.960	90	1.014	Lower
2	1.443	80	.990	
3	1.409	70	.987	
4	1.379	60	.986	
5	1.436	50	.988	
6	1.367	40	.978	
7	1.371	30	.955	
8	1.341	20	.878	
9	1.382	15	1.476	Upper
10	1.338	25	1.454	
11	1.357	35	1.468	
12	1.356	45	1.411	
13	1.336	55	1.421	
14	1.287	65	1.421	
15	1.241	75	1.300	
16	-----	85	1.185	
17	-----	95	1.190	

(c)

Wall orifice	M_1	Station, percent c	M_b	
(c) $\frac{\Delta p_t}{q_1} = 0.0777$; $\bar{M}_1 = 1.389$, $\bar{M}_2 = 1.058$				
1	1.053	90	1.012	Lower
2	1.410	80	.966	
3	1.451	70	.926	
4	1.453	60	.891	
5	1.469	50	.980	
6	1.370	40	1.274	
7	1.422	30	1.319	
8	1.389	20	1.333	
9	1.395	15	1.472	Upper
10	1.416	25	1.401	
11	1.420	35	1.354	
12	1.420	45	1.365	
13	-----	55	1.410	
14	-----	65	1.461	
15	-----	75	1.396	
16	-----	85	1.317	
17	-----	95	1.323	

(d)

Wall orifice	M_1	Station, percent c	M_b	
(d) $\frac{\Delta p_t}{q_1} = 0.0819$; $\bar{M}_1 = 1.419$, $\bar{M}_2 = 1.052$				
1	1.045	90	1.026	Lower
2	1.440	80	.997	
3	1.500	70	.970	
4	1.466	60	.926	
5	1.419	50	.886	
6	1.447	40	.935	
7	1.484	30	1.244	
8	1.412	20	1.336	
9	1.461	15	1.601	Upper
10	1.452	25	1.598	
11	1.458	35	1.582	
12	1.438	45	1.589	
13	-----	55	1.518	
14	-----	65	1.486	
15	-----	75	1.602	
16	-----	85	1.339	
17	-----	95	1.345	

L-59-6055

Figure 17.- Schlieren photographs and Mach number distribution from cascade tests of CW_1 blade sections at $\alpha = 2^\circ$, $\beta = 52^\circ$, and $\sigma = 0.80$.

	Wall orifice	M_1	Station, percent c	M_b	
(a)	$\frac{\Delta p_t}{q_1} = 0.0998$; $\bar{M}_1 = 1.347$; $\bar{M}_2 = 0.996$				
	1	0.981	90	1.031	Lower
	2	1.385	80	1.008	
	3	1.500	70	.999	
	4	1.488	60	.999	
	5	1.508	50	.998	
	6	1.496	40	.989	
	7	1.458	30	.947	
	8	1.381	20	.893	
	9	1.591	15	1.464	Upper
	10	1.567	25	1.424	
	11	1.547	35	1.447	
	12	1.541	45	1.482	
	13	1.511	55	1.487	
	14	1.264	65	1.300	
	15	1.199	75	1.307	
	16	1.144	85	1.237	
	17	-----	95	1.242	
(b)	$\frac{\Delta p_t}{q_1} = 0.0870$; $\bar{M}_1 = 1.338$; $\bar{M}_2 = 0.997$				
	1	0.982	90	1.011	Lower
	2	1.326	80	.986	
	3	1.419	70	.971	
	4	1.460	60	.955	
	5	1.498	50	.944	
	6	1.496	40	.918	
	7	1.480	30	.893	
	8	1.439	20	.860	
	9	1.369	15	1.533	Upper
	10	1.334	25	1.558	
	11	1.511	35	1.576	
	12	1.502	45	1.605	
	13	1.269	55	1.575	
	14	1.227	65	1.535	
	15	1.165	75	1.324	
	16	1.106	85	1.284	
	17	-----	95	1.282	
(c)	$\frac{\Delta p_t}{q_1} = 0.0846$; $\bar{M}_1 = 1.372$; $\bar{M}_2 = 1.036$				
	1	1.024	90	1.026	Lower
	2	1.396	80	1.000	
	3	1.522	70	.980	
	4	1.493	60	.951	
	5	1.513	50	.912	
	6	1.519	40	.886	
	7	1.482	30	.992	
	8	1.405	20	1.318	Upper
	9	1.389	15	1.389	
	10	1.363	25	1.400	
	11	1.355	35	1.442	
	12	1.340	45	1.480	
	13	1.315	55	1.496	
	14	1.265	65	1.535	
	15	1.203	75	1.482	
	16	-----	85	1.351	
	17	-----	95	1.343	
(d)	$\frac{\Delta p_t}{q_1} = 0.0898$; $\bar{M}_1 = 1.396$; $\bar{M}_2 = 1.036$				
	1	1.021	90	1.052	Lower
	2	1.523	80	1.033	
	3	1.565	70	1.033	
	4	1.503	60	1.036	
	5	1.524	50	1.019	
	6	1.495	40	.982	
	7	1.413	30	.907	
	8	1.434	20	.918	
	9	1.426	15	1.516	Upper
	10	1.417	25	1.548	
	11	1.393	35	1.545	
	12	1.378	45	1.563	
	13	1.342	55	1.541	
	14	1.297	65	1.516	
	15	1.227	75	1.585	
	16	-----	85	1.300	
	17	-----	95	1.302	

L-59-6056

Figure 18.- Schlieren photographs and Mach number distribution from cascade tests of CW_1 blade sections at $\alpha = 4^\circ$, $\beta = 54^\circ$, and $\sigma = 0.80$.

(a)

Wall orifice	M_1	Station, percent c	M_b	
(a) $\frac{\Delta p_t}{q_1} = 0.0765$; $\bar{M}_1 = 1.161$; $\bar{M}_2 = 0.897$				
1	0.885	90	0.969	Lower
2	1.182	80	.943	
3	1.195	70	.928	
4	1.096	60	.917	
5	1.170	50	.904	
6	1.238	40	.899	
7	1.183	30	.865	
8	1.128	20	.820	
9	1.187	15	1.505	Upper
10	1.262	25	1.462	
11	1.232	35	1.448	
12	1.182	45	1.436	
13	1.172	55	1.333	
14	1.213	65	1.117	
15	1.164	75	1.071	
16	1.085	85	1.055	
17	-----	95	1.055	

(b)

Wall orifice	M_1	Station, percent c	M_b	
(b) $\frac{\Delta p_t}{q_1} = 0.1036$; $\bar{M}_1 = 1.113$; $\bar{M}_2 = 0.884$				
1	0.877	90	0.953	Lower
2	1.113	80	.923	
3	1.212	70	.909	
4	1.090	60	.900	
5	1.081	50	.895	
6	1.269	40	.892	
7	1.186	30	.865	
8	1.084	20	.818	
9	1.167	15	1.571	Upper
10	1.246	25	1.452	
11	1.182	35	1.259	
12	1.079	45	1.141	
13	1.042	55	1.116	
14	1.082	65	1.097	
15	1.074	75	1.081	
16	1.028	85	1.072	
17	-----	95	1.070	

(c)

Wall orifice	M_1	Station, percent c	M_b	
(c) $\frac{\Delta p_t}{q_1} = 0.1078$; $\bar{M}_1 = 1.269$; $\bar{M}_2 = 0.964$				
1	0.952	90	1.002	Lower
2	1.292	80	.971	
3	1.267	70	.956	
4	1.266	60	.946	
5	1.420	50	.942	
6	1.458	40	.941	
7	1.441	30	.915	
8	1.415	20	.876	
9	1.342	15	1.552	Upper
10	1.264	25	1.573	
11	1.216	35	1.587	
12	1.235	45	1.456	
13	1.259	55	1.242	
14	1.225	65	1.228	
15	1.169	75	1.225	
16	1.109	85	1.225	
17	-----	95	1.217	

(d)

Wall orifice	M_1	Station, percent c	M_b	
(d) $\frac{\Delta p_t}{q_1} = 0.1131$; $\bar{M}_1 = 1.286$; $\bar{M}_2 = 0.959$				
1	0.945	90	1.004	Lower
2	1.322	80	.976	
3	1.298	70	.963	
4	1.361	60	.959	
5	1.448	50	.956	
6	1.438	40	.958	
7	1.435	30	.928	
8	1.390	20	.882	
9	1.315	15	1.486	Upper
10	1.282	25	1.501	
11	1.251	35	1.526	
12	1.277	45	1.546	
13	1.282	55	1.438	
14	1.239	65	1.202	
15	1.175	75	1.186	
16	1.118	85	1.187	
17	-----	95	1.188	

L-59-6057

Figure 19.- Schlieren photographs and Mach number distribution from cascade tests of CW_1 blade sections at $\alpha = 4^\circ$, $\beta = 54^\circ$, and $\sigma = 0.80$.

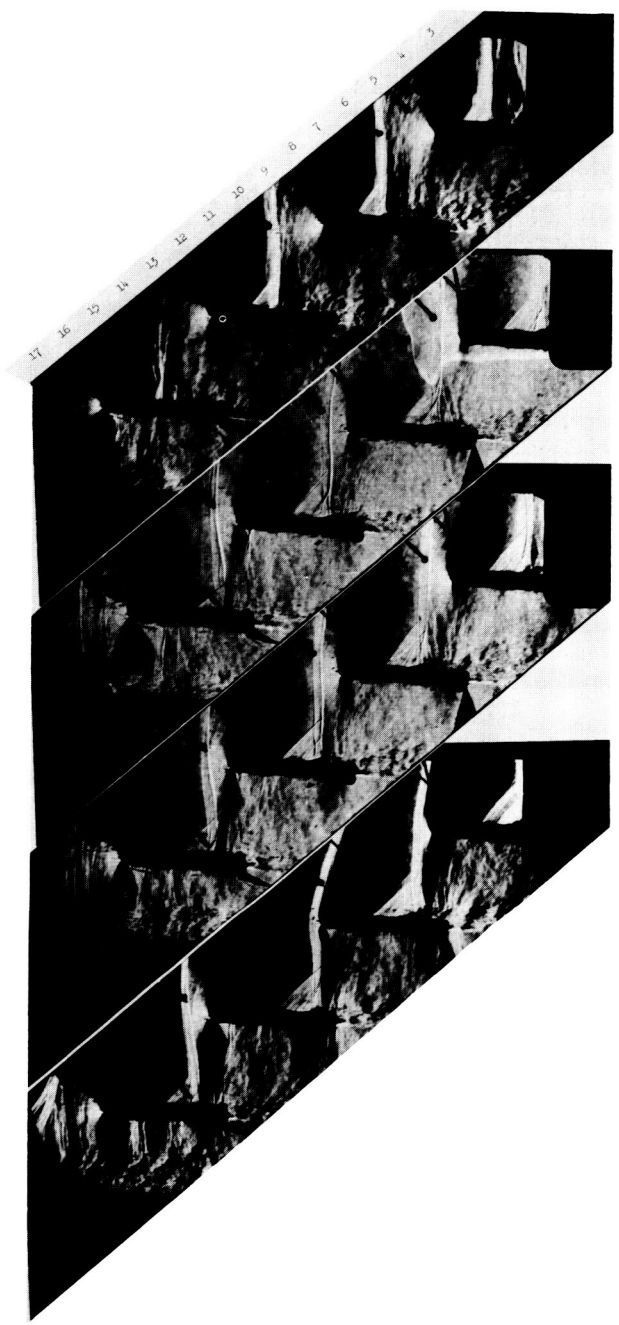

	Wall orifice	M_1	Station, percent c	M_b
(a)	$\frac{\Delta p_t}{q_1}$ = 0.0548; $\bar{M}_1$ = 0.953; $\bar{M}_2$ = 0.743			
	1	0.916		
	2	1.082		
	3	.992		
	4	.909		
	5	.966		
	6	1.070		
	7	.897		
	8	.888		
	9	.949		
	10	1.019		
	11	.955		
	12	.887		
	13	.907		
	14	.943		
	15	.942		
	16	.923		
	17	-----		
(b)	$\frac{\Delta p_t}{q_1}$ = 0.0512; $\bar{M}_1$ = 1.033; $\bar{M}_2$ = 0.820			
	1	1.023		
	2	1.117		
	3	1.018		
	4	1.053		
	5	1.143		
	6	1.075		
	7	.941		
	8	1.054		
	9	1.111		
	10	1.044		
	11	.966		
	12	.974		
	13	1.040		
	14	1.024		
	15	.986		
	16	.967		
	17	-----		
(c)	$\frac{\Delta p_t}{q_1}$ = 0.0656; $\bar{M}_1$ = 1.038; $\bar{M}_2$ = 0.820			
	1	1.005		
	2	1.132		
	3	1.021		
	4	1.012		
	5	1.159		
	6	1.100		
	7	.948		
	8	1.047		
	9	1.140		
	10	1.074		
	11	.995		
	12	.973		
	13	1.026		
	14	1.021		
	15	.994		
	16	.962		
	17	-----		
(d)	$\frac{\Delta p_t}{q_1}$ = 0.0607; $\bar{M}_1$ = 1.093; $\bar{M}_2$ = 0.873			
	1	1.055		
	2	1.148		
	3	1.070		
	4	1.191		
	5	1.194		
	6	1.137		
	7	1.049		
	8	1.198		
	9	1.128		
	10	1.052		
	11	.981		
	12	1.012		
	13	1.084		
	14	1.070		
	15	1.044		
	16	1.038		
	17	-----		

L-59-6058

Figure 20.- Schlieren photographs and Mach number distribution from cascade tests of 65-$(4A_{10})06$ blade sections at $\alpha = 2^\circ$, $\beta = 50^\circ$, and $\sigma = 0.80$.

Wall orifice	M_1	Station, percent c	M_b
(a) $\frac{\Delta p_t}{q_1} = 0.0614$; $\bar{M}_1 = 1.114$, $\bar{M}_2 = 0.901$			
1	1.181		
2	1.151		
3	1.105		
4	1.229		
5	1.204		
6	1.159		
7	1.069		
8	1.179		
9	1.104		
10	1.037		
11	.983		
12	1.065		
13	1.134		
14	1.102		
15	1.062		
16	1.057		
17	-----		
(b) $\frac{\Delta p_t}{q_1} = 0.0673$; $\bar{M}_1 = 1.144$, $\bar{M}_2 = 0.929$			
1	1.231		
2	1.171		
3	1.180		
4	1.264		
5	1.202		
6	1.123		
7	1.019		
8	1.152		
9	1.106		
10	1.072		
11	1.087		
12	1.135		
13	1.178		
14	1.133		
15	1.084		
16	1.108		
17	-----		
(c) $\frac{\Delta p_t}{q_1} = 0.0686$; $\bar{M}_1 = 1.105$, $\bar{M}_2 = 0.965$			
1	1.208		
2	1.159		
3	1.170		
4	1.232		
5	1.185		
6	1.126		
7	1.079		
8	1.203		
9	1.134		
10	1.051		
11	.983		
12	1.055		
13	1.072		
14	1.051		
15	.991		
16	1.005		
17	-----		
(d) $\frac{\Delta p_t}{q_1} = 0.0598$; $\bar{M}_1 = 1.112$, $\bar{M}_2 = 0.992$			
1	1.219		
2	1.159		
3	1.188		
4	1.242		
5	1.191		
6	1.138		
7	1.079		
8	1.192		
9	1.119		
10	1.076		
11	.966		
12	1.040		
13	1.088		
14	1.060		
15	1.025		
16	1.049		
17	-----		

L-59-6059

Figure 21.- Schlieren photographs and Mach number distribution from cascade tests of 65-$(4A_{10})$06 blade sections at $\alpha = 2^\circ$, $\beta = 50^\circ$, and $\sigma = 0.80$.

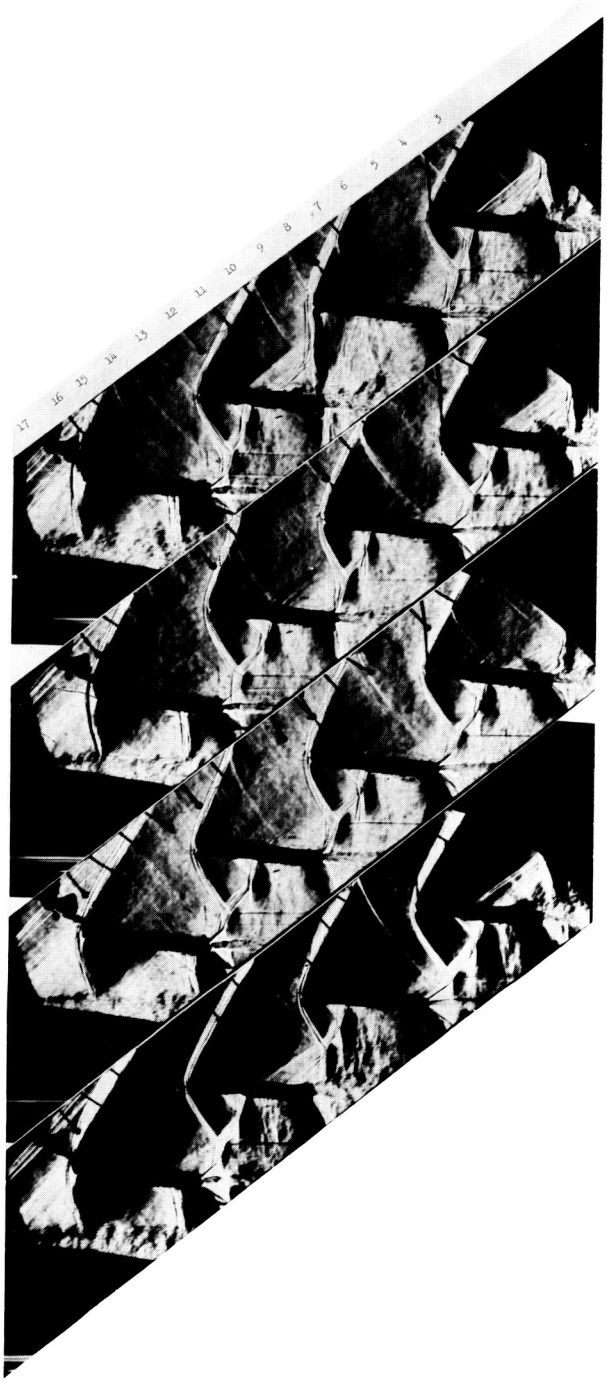

	Wall orifice	M_1	Station, percent c	M_b
(a)	$\frac{\Delta p_t}{q_1} = 0.0806$; $\bar{M}_1 = 1.222$; $\bar{M}_2 = 0.974$			
	1	1.307		
	2	1.220		
	3	1.262		
	4	1.259		
	5	1.246		
	6	1.181		
	7	1.081		
	8	1.240		
	9	1.209		
	10	1.182		
	11	1.233		
	12	1.285		
	13	1.254		
	14	1.208		
	15	1.166		
	16	1.213		
	17	-----		
(b)	(b) $\frac{\Delta p_t}{q_1} = 0.0720$; $\bar{M}_1 = 1.194$; $\bar{M}_2 = 1.005$			
	1	1.291		
	2	1.218		
	3	1.226		
	4	1.269		
	5	1.193		
	6	1.172		
	7	1.098		
	8	1.184		
	9	1.137		
	10	1.110		
	11	1.141		
	12	1.245		
	13	1.221		
	14	1.193		
	15	1.206		
	16	-----		
	17	-----		
(c)	(c) $\frac{\Delta p_t}{q_1} = 0.0725$; $\bar{M}_1 = 1.205$; $\bar{M}_2 = 1.028$			
	1	1.297		
	2	1.214		
	3	1.219		
	4	1.260		
	5	1.169		
	6	1.177		
	7	1.088		
	8	1.186		
	9	1.165		
	10	1.129		
	11	1.174		
	12	1.261		
	13	1.254		
	14	1.225		
	15	1.254		
	16	-----		
	17	-----		
(d)	(d) $\frac{\Delta p_t}{q_1} = 0.0588$; $\bar{M}_1 = 1.241$; $\bar{M}_2 = 1.032$			
	1	1.309		
	2	1.212		
	3	1.218		
	4	1.269		
	5	1.238		
	6	1.163		
	7	1.156		
	8	1.272		
	9	1.252		
	10	1.298		
	11	1.287		
	12	1.315		
	13	1.273		
	14	1.227		
	15	1.233		
	16	-----		
	17	-----		

L-59-6060

Figure 22.- Schlieren photographs and Mach number distribution from cascade tests of 65-$(4A_{10})$06 blade sections at $\alpha = 4^\circ$, $\beta = 52^\circ$, and $\sigma = 0.80$.

(a)

Wall orifice	M_1	Station, percent c	M_b
(a) $\frac{\Delta p_t}{q_1} = 0.0608$; $\bar{M}_1 = 1.041$, $\bar{M}_2 = 0.789$			
1	0.988		
2	1.136		
3	1.050		
4	.988		
5	1.094		
6	1.111		
7	.966		
8	1.029		
9	1.151		
10	1.060		
11	.978		
12	.977		
13	1.043		
14	1.034		
15	1.021		
16	1.047		
17	-----		

(b)

(b) $\frac{\Delta p_t}{q_1} = 0.0717$; $\bar{M}_1 = 1.120$, $\bar{M}_2 = 0.870$			
1	1.104		
2	1.177		
3	1.077		
4	1.154		
5	1.213		
6	1.164		
7	1.083		
8	1.231		
9	1.156		
10	1.070		
11	1.006		
12	1.067		
13	1.126		
14	1.106		
15	1.077		
16	1.103		
17	-----		

(c)

(c) $\frac{\Delta p_t}{q_1} = 0.0725$; $\bar{M}_1 = 1.153$, $\bar{M}_2 = 0.909$			
1	1.188		
2	1.184		
3	1.116		
4	1.245		
5	1.245		
6	1.181		
7	1.126		
8	1.214		
9	1.140		
10	1.066		
11	1.029		
12	1.156		
13	1.174		
14	1.140		
15	1.104		
16	1.133		
17	-----		

(d)

(d) $\frac{\Delta p_t}{q_1} = 0.0787$; $\bar{M}_1 = 1.206$, $\bar{M}_2 = 0.942$			
1	1.284		
2	1.218		
3	1.259		
4	1.279		
5	1.212		
6	1.188		
7	1.083		
8	1.196		
9	1.189		
10	1.166		
11	1.199		
12	1.270		
13	1.238		
14	1.194		
15	1.147		
16	1.181		
17	-----		

L-59-6061

Figure 23.- Schlieren photographs and Mach number distribution from cascade tests of 65-$(4A_{10})$06 blade sections at $\alpha = 4^\circ$, $\beta = 52^\circ$, and $\sigma = 0.80$.

(a)

Wall orifice	M_1	Station, percent c	M_b
(a) $\frac{\Delta p_t}{q_1}$ = 0.0693; $\bar{M}_1$ = 1.036, $\bar{M}_2$ = 0.795			
1	0.946		
2	1.089		
3	1.062		
4	.973		
5	1.052		
6	1.146		
7	.975		
8	.976		
9	1.136		
10	1.115		
11	1.021		
12	.981		
13	1.050		
14	1.049		
15	1.017		
16	.992		
17	-----		

(b)

(b) $\frac{\Delta p_t}{q_1}$ = 0.0869; $\bar{M}_1$ = 1.145, $\bar{M}_2$ = 0.884			
1	1.093		
2	1.207		
3	1.099		
4	1.096		
5	1.240		
6	1.202		
7	1.107		
8	1.283		
9	1.215		
10	1.122		
11	1.052		
12	1.091		
13	1.165		
14	1.147		
15	1.107		
16	1.088		
17	-----		

(c)

(c) $\frac{\Delta p_t}{q_1}$ = 0.0960; $\bar{M}_1$ = 1.227, $\bar{M}_2$ = 0.953			
1	1.251		
2	1.238		
3	1.183		
4	1.330		
5	1.286		
6	1.256		
7	1.166		
8	1.267		
9	1.224		
10	1.187		
11	1.197		
12	1.283		
13	1.264		
14	1.205		
15	1.150		
16	1.145		
17	-----		

(d)

(d) $\frac{\Delta p_t}{q_1}$ = 0.0883; $\bar{M}_1$ = 1.262, $\bar{M}_2$ = 0.984			
1	1.318		
2	1.272		
3	1.318		
4	1.332		
5	1.310		
6	1.238		
7	1.142		
8	1.299		
9	1.264		
10	1.233		
11	1.282		
12	1.326		
13	1.283		
14	1.232		
15	1.175		
16	1.171		
17	-----		

L-59-6062

Figure 24.- Schlieren photographs and Mach number distribution from cascade tests of 65-$(4A_{10})$06 blade sections at $\alpha = 6^\circ$, $\beta = 54^\circ$, and $\sigma = 0.80$.

	Wall orifice	M_1	Station, percent c	M_b
	(a) $\frac{\Delta p_t}{q_1} = 0.1025$;		$\bar{M}_1 = 1.280$; $\bar{M}_2 = 1.007$	
(a)	1	1.320		
	2	1.287		
	3	1.337		
	4	1.324		
	5	1.308		
	6	1.208		
	7	1.150		
	8	1.312		
	9	1.281		
	10	1.271		
	11	1.347		
	12	1.336		
	13	1.300		
	14	1.242		
	15	1.184		
	16	-----		
	17	-----		
	(b) $\frac{\Delta p_t}{q_1} = 0.0869$;		$\bar{M}_1 = 1.265$; $\bar{M}_2 = 1.036$	
(b)	1	1.322		
	2	1.285		
	3	1.318		
	4	1.309		
	5	1.290		
	6	1.244		
	7	1.159		
	8	1.263		
	9	1.236		
	10	1.206		
	11	1.309		
	12	1.317		
	13	1.281		
	14	1.238		
	15	1.204		
	16	-----		
	17	-----		
	(c) $\frac{\Delta p_t}{q_1} = 0.0877$;		$\bar{M}_1 = 1.325$; $\bar{M}_2 = 1.071$	
(c)	1	1.319		
	2	1.310		
	3	1.346		
	4	1.361		
	5	1.288		
	6	1.297		
	7	1.257		
	8	1.347		
	9	1.324		
	10	1.352		
	11	1.401		
	12	1.378		
	13	1.339		
	14	1.285		
	15	1.275		
	16	-----		
	17	-----		
	(d) $\frac{\Delta p_t}{q_1} = 0.0739$;		$\bar{M}_1 = 1.284$; $\bar{M}_2 = 1.070$	
(d)	1	1.346		
	2	1.287		
	3	1.313		
	4	1.302		
	5	1.302		
	6	1.229		
	7	1.191		
	8	1.283		
	9	1.242		
	10	1.262		
	11	1.348		
	12	1.342		
	13	1.302		
	14	1.263		
	15	1.254		
	16	-----		
	17	-----		

L-59-6063

Figure 25.- Schlieren photographs and Mach number distribution from cascade tests of 65-$(4A_{10})$06 blade sections at $\alpha = 6^\circ$, $\beta = 54^\circ$, and $\sigma = 0.80$.

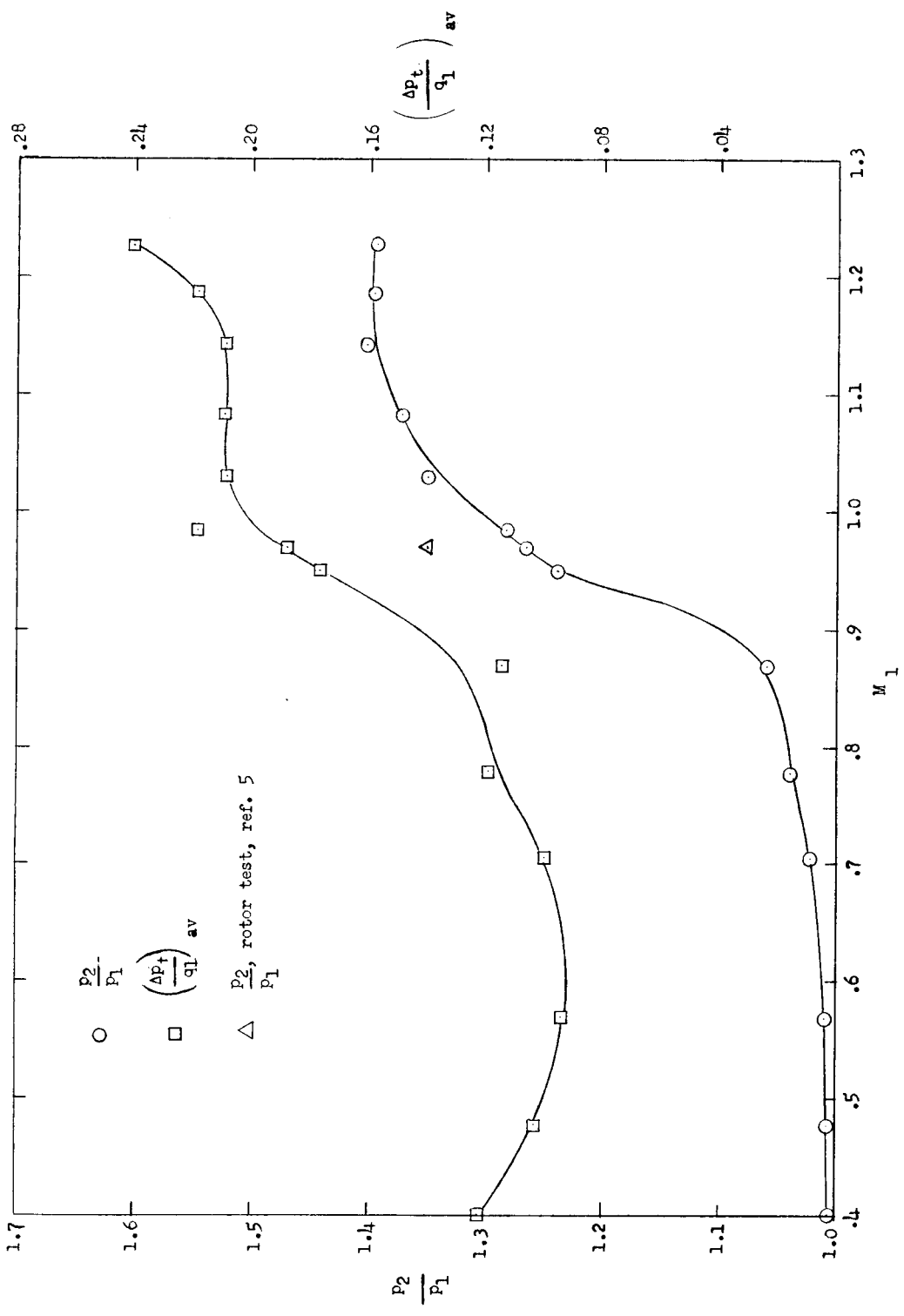

Figure 26.- Pressure ratio and total-pressure-loss coefficient plotted against Mach number for the T1-$(8A_2I_{8_b})$06 blade section at $\alpha = 13.6^\circ$, $\beta = 56.1^\circ$, and $\sigma = 0.80$.

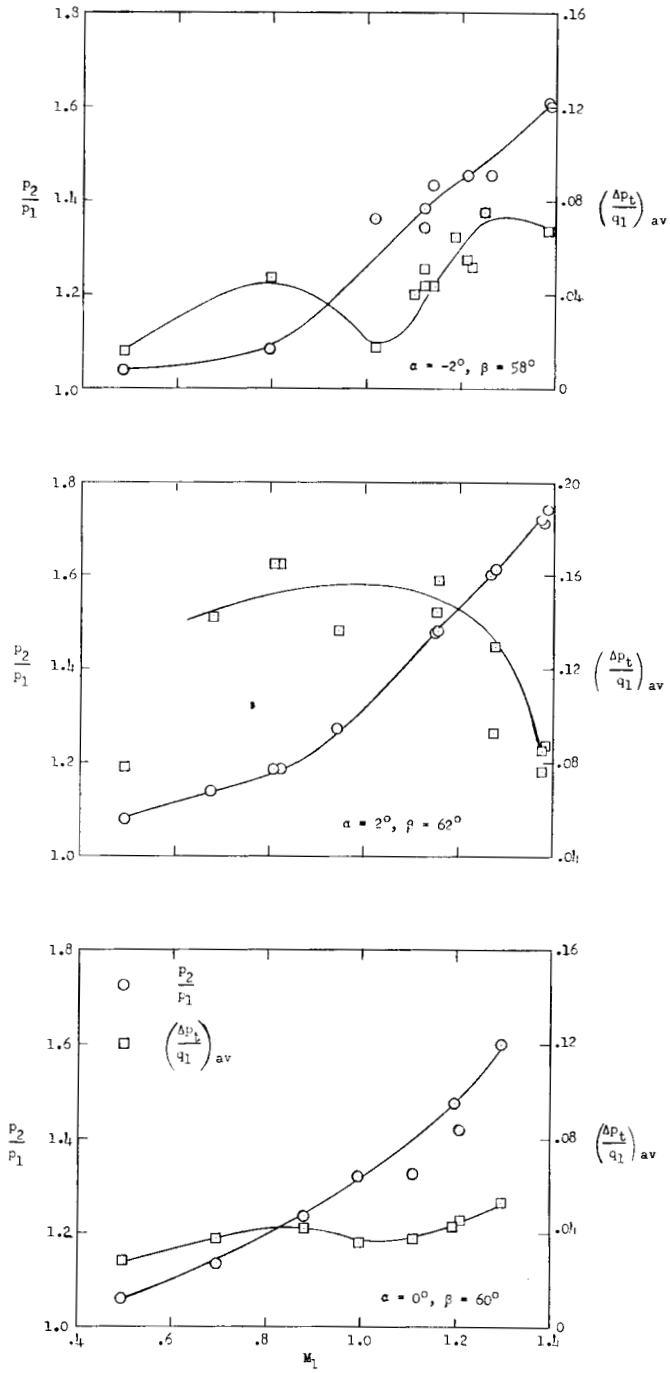

Figure 27.- Pressure ratio and total-pressure-loss coefficient plotted against Mach number for the CW_1 blade section at $\alpha = 0^\circ$, $\beta = 60^\circ$; $\alpha = 2^\circ$, $\beta = 62^\circ$; and $\alpha = -2^\circ$, $\beta = 58^\circ$. $\sigma = 0.80$.

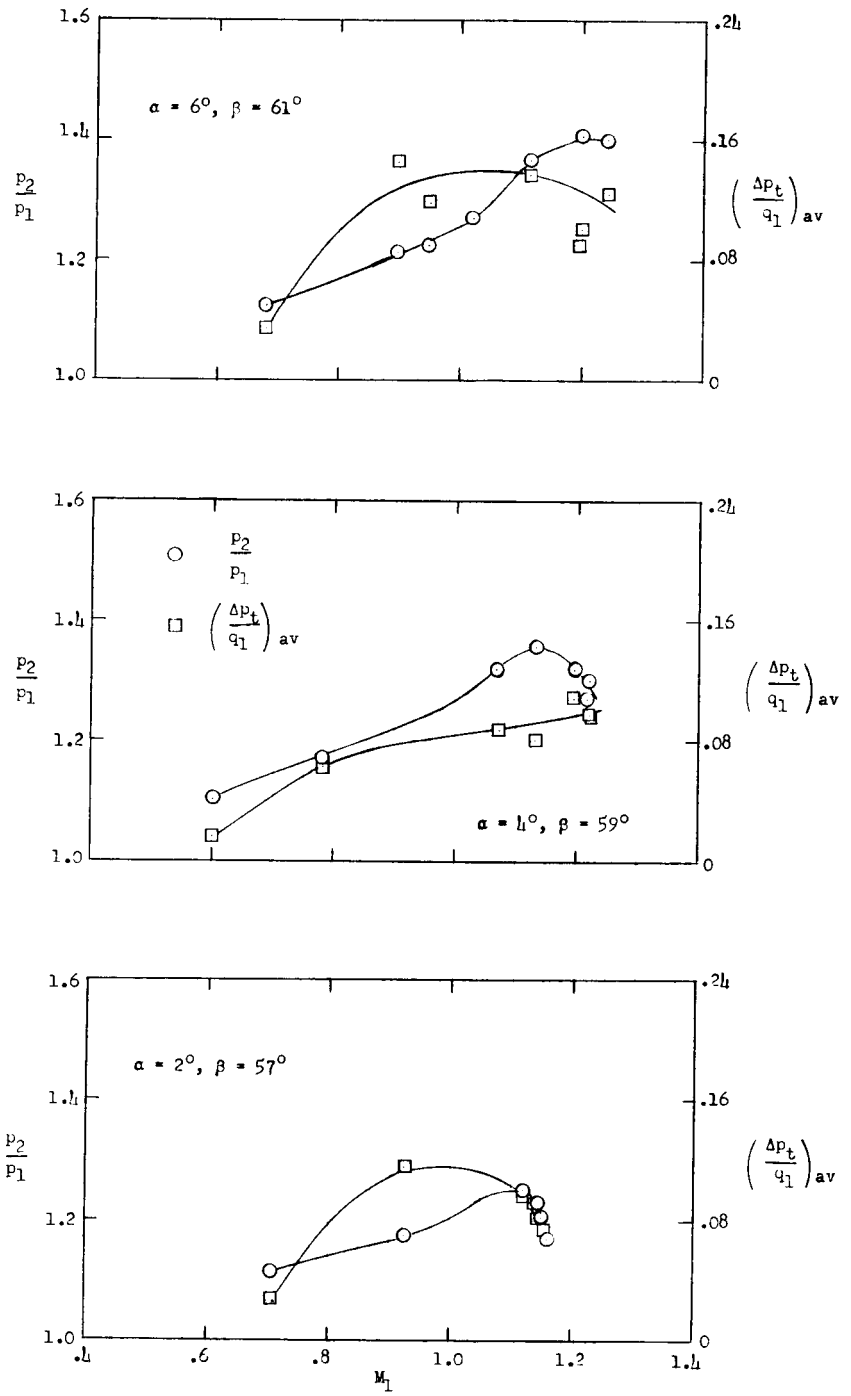

Figure 28.- Pressure ratio and total-pressure-loss coefficient plotted against Mach number for the CW_2 blade section at $\alpha = 2^\circ$, $\beta = 57^\circ$; $\alpha = 4^\circ$, $\beta = 59^\circ$; and $\alpha = 6^\circ$, $\beta = 61^\circ$. $\sigma = 0.80$.

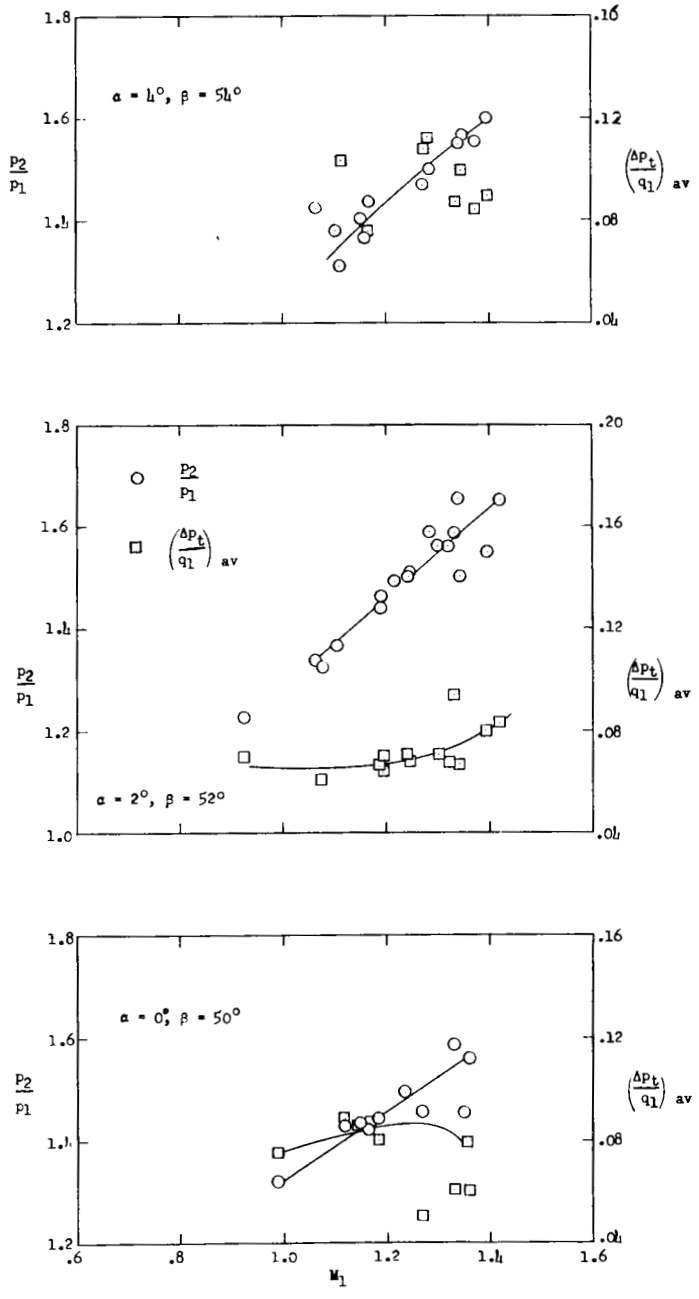

Figure 29.- Pressure ratio and total-pressure-loss coefficient plotted against Mach number for the CW_1 blade section at $\alpha = 0^\circ$, $\beta = 50^\circ$; $\alpha = 2^\circ$, $\beta = 52^\circ$; and $\alpha = 4^\circ$, $\beta = 54^\circ$. $\sigma = 0.80$.

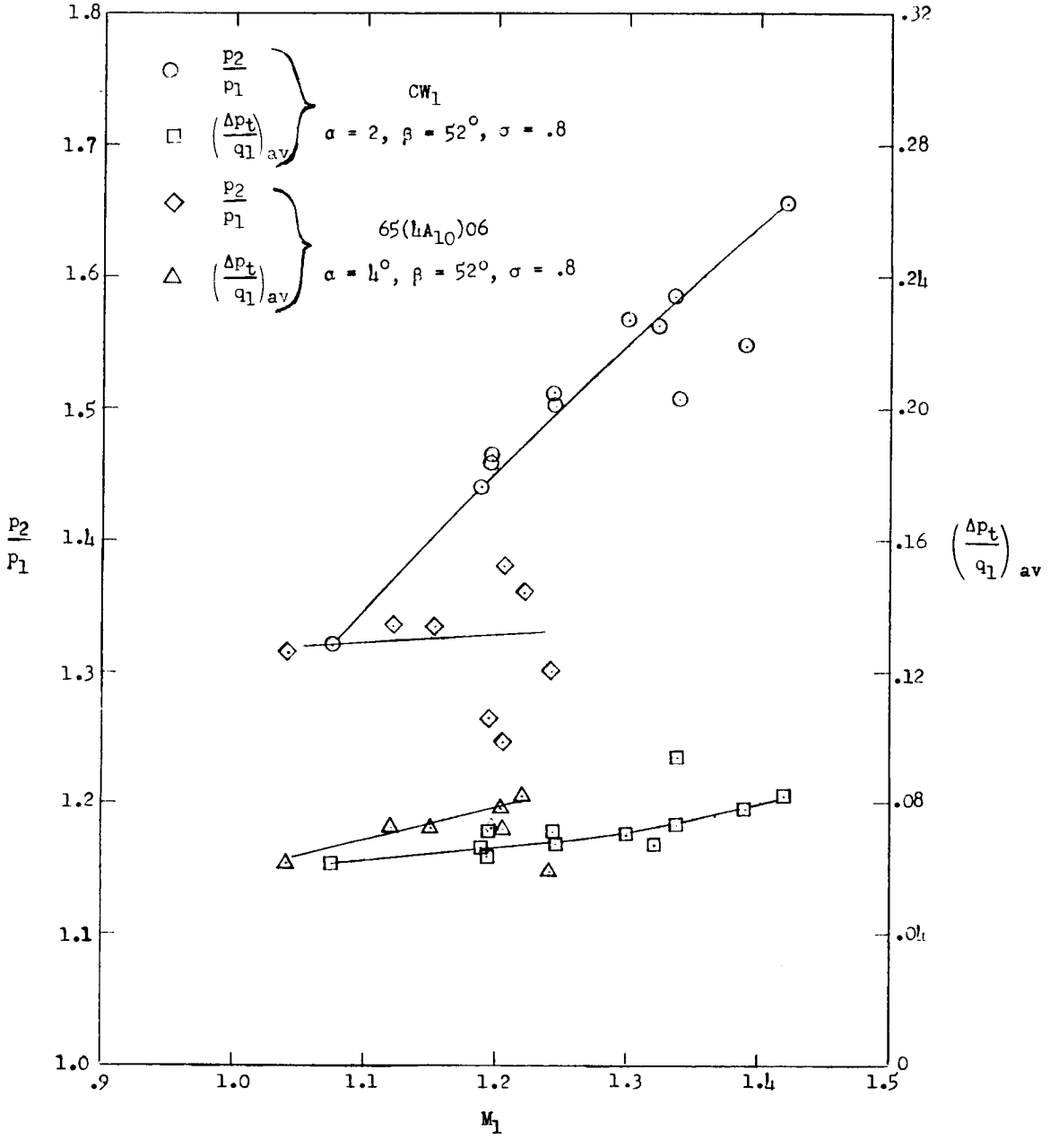

Figure 30.- Comparison of pressure ratio and total-pressure-loss coefficient for the CW_1 and $65\text{-}(4A_{10})06$ blade sections at several Mach numbers.